Volume 54
Number 19
7 October 2025
Pages 8527–9118

Chem Soc Rev

Chemical Society Reviews

rsc.li/chem-soc-rev

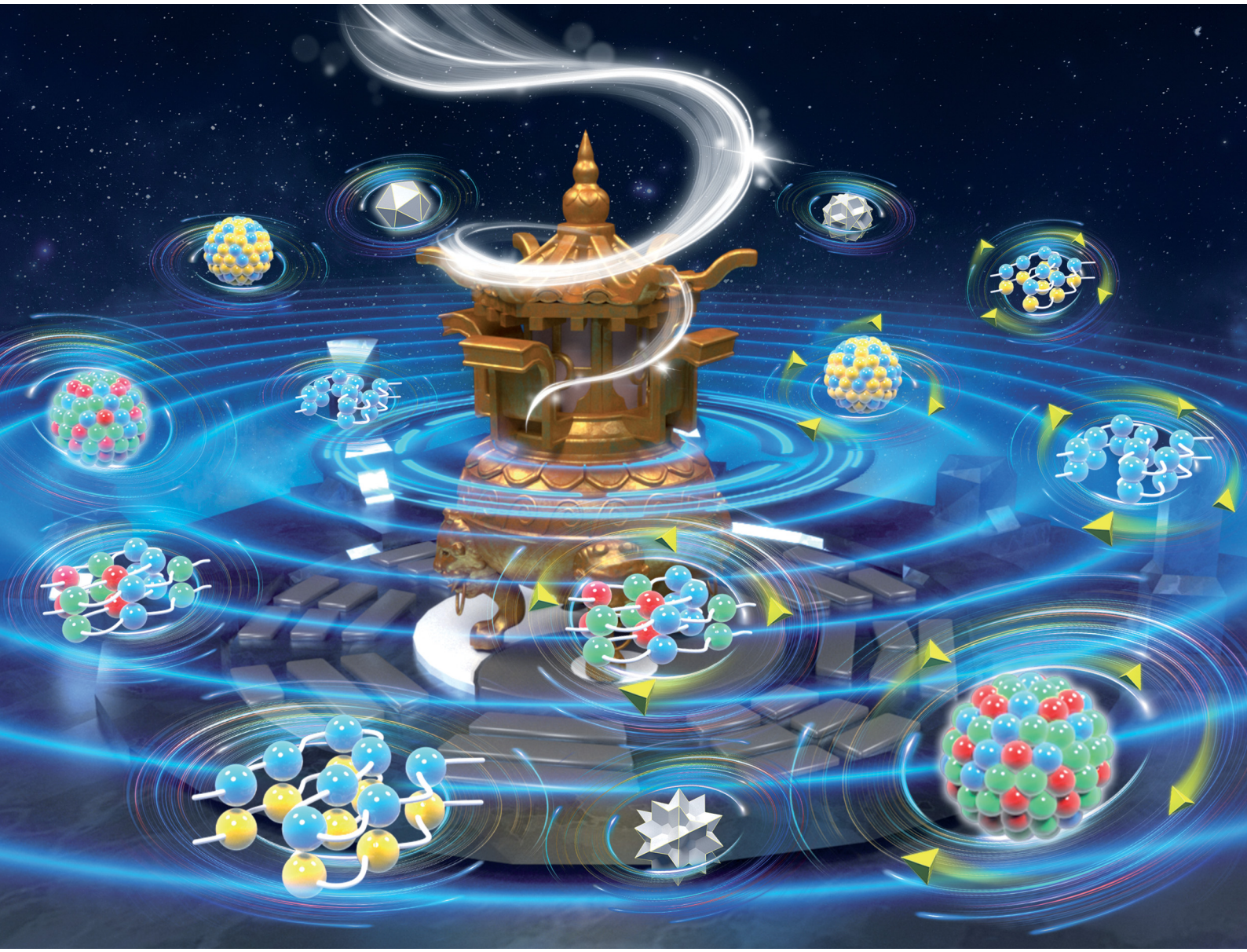

ISSN 0306-0012

ROYAL SOCIETY OF CHEMISTRY

TUTORIAL REVIEW

Hai-Yan Lu, Chuan-Feng Chen *et al.*

Recent advances in preparation and applications of white circularly polarized luminescent materials

Chem Soc Rev

TUTORIAL REVIEW

View Article Online
View Journal | View Issue

Cite this: *Chem. Soc. Rev.*, 2025, **54**, 8534

Recent advances in preparation and applications of white circularly polarized luminescent materials

Pei Zhao,[ab] Hai-Yan Lu*[a] and Chuan-Feng Chen *[ab]

White circularly polarized luminescence (WCPL) integrates the characteristics of circular polarization luminescence and broadband white emission, enabling chiroptical luminescence under photoexcitation or electroluminescence conditions. Recently, WCPL materials have attracted increasing attention from both academic and industrial communities due to their potential applications in a wide range of fields, including optical anti-counterfeiting, information storage, biomedical diagnostics, optical sensing, and next-generation optoelectronic devices. In this review, we systematically summarize recent advances in the design, synthesis, and application of WCPL-active materials. Particular emphasis is placed on three representative designing strategies of WCPL materials: polymer-based systems, multicomponent-doped systems and single-component systems. These approaches collectively highlight the diverse molecular design principles and structure–property relationships underlying efficient WCPL behavior. We believe that this review will provide valuable insights for researchers across various disciplines and inspire further exploration and innovation in this rapidly evolving field of chiral luminescent materials.

Received 24th June 2025

DOI: 10.1039/d5cs00410a

rsc.li/chem-soc-rev

Key learning points
(1) Fundamental concepts of white circularly polarized luminescence.
(2) Characterization methods for white circularly polarized luminescence.
(3) Design strategies for white circularly polarized luminescent materials.
(4) Current development status of white circularly polarized luminescent materials.
(5) Future challenges of white circularly polarized luminescent materials.

1. Introduction

Circularly polarized (CP) light is a specific type of polarized light in which the electromagnetic vector rotates continuously with constant amplitude in a plane perpendicular to the direction of propagation, forming a helical wavefront.[1] Depending on the rotation direction of the electromagnetic vector, CPL can be classified as right-handed CP light (R-CP light) or left-handed CP light (L-CP light). When the electromagnetic vector rotates clockwise along the direction of propagation from the receiver's perspective, the light is designated as R-CP light; conversely, counterclockwise rotation corresponds to L-CP light (Fig. 1).[2] When CP light is directly emitted from the excited state of chiral luminescent materials, the process is referred to as circularly polarized luminescence (CPL). The chiroptical activity of such emission can be quantitatively evaluated using the luminescence dissymmetry factor ($|g_{lum}|$), which is defined as $|g_{lum}| = 2|I_L - I_R|/(I_L + I_R)$, where I_L and I_R represent the emission intensities of left-handed and right-handed circularly polarized light, respectively.[3–5] Theoretically, the magnitude of $|g_{lum}|$ ranges from 0 to 2, with higher values indicating an increased degree of circular polarization in the emitted light.[6]

White light is composite emission covering a broad spectrum of visible wavelengths, typically ranging from 400 to 700 nm.[7] In the context of optoelectronic functional materials,

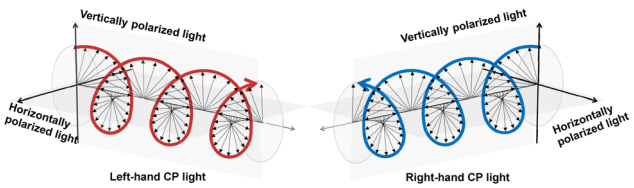

Fig. 1 Schematic illustration of right-handed and left-handed CP light.

[a] University of Chinese Academy of Sciences, Beijing 100049, China. E-mail: haiyanlu@ucas.ac.cn, cchen@iccas.ac.cn
[b] Beijing National Laboratory for Molecular Sciences, CAS Key Laboratory of Molecular Recognition and Function, Institute of Chemistry, Chinese Academy of Sciences, Beijing 100190, China

white-emission performance serves as a critical parameter for assessing practical applicability. Its evaluation involves a comprehensive consideration of several key metrics, including the Commission Internationale de l'Eclairage (CIE) coordinates, color rendering index (CRI), and correlated color temperature (CCT).[8] These parameters collectively provide insights into spectral continuity, color fidelity, and visual comfort, thereby enabling a systematic assessment of the suitability of white-emissive systems for advanced lighting and display applications.

White circularly polarized luminescence (WCPL) integrates the characteristics of both circular polarization and broadband white emission, enabling chiroptical luminescence under photoexcitation or electroluminescence conditions. Recently, WCPL materials have attracted significant attention in both academic and industrial fields owing to their promising applications in several cutting-edge areas, including optical anti-counterfeiting, information storage, biomedical field, optical sensing and optoelectronic devices.[9–15] Currently, the design strategies for WCPL materials can be broadly categorized into three main approaches: (i) polymer-based systems engineered to exhibit WCPL emission; (ii) multicomponent doped composites integrating multiple emissive and chiral components; and (iii) single-component luminophores that intrinsically exhibit both white-light emission and circularly polarized luminescence properties (Fig. 2).

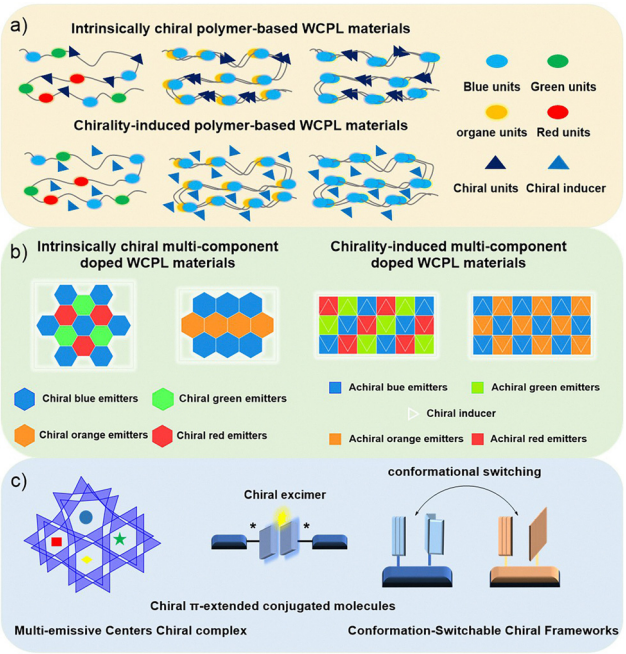

Fig. 2 (a) Polymer-based WCPL materials. (b) Multicomponent-doped WCPL materials. (c) Single-component WCPL materials.

Based on these strategies, WCPL-active material systems have been successfully developed, including macrocyclic compounds,[16] liquid crystal complexes,[17,18] quantum dots,[19] nanoparticles,[20] polymers,[21,22] organic–inorganic hybrid perovskite materials,[23,24] metal complexes,[25] and microcrystals.[26] Despite rapid progress, a comprehensive and systematic overview that summarizes designing strategies, deciphers structure–property correlations, and delineates future directions remains lacking. In this review, we critically summarize recent developments in the field of WCPL materials, emphasizing molecular-level design principles and multiscale assembly strategies across various material classes. Particular attention is given to the interplay among molecular chirality, supramolecular organization and photophysical behavior. We believe that

Pei Zhao

Pei Zhao received her MS degree from the University of Shan Dong in 2021. She is currently pursuing her PhD at the University of Chinese Academy of Sciences under the supervision of Prof. Hai-Yan Lu and Prof Chuan-Feng Chen. Her research focuses on the synthesis and application of white circularly polarized luminescent materials.

Hai-Yan Lu

Hai-Yan Lu received her PhD from the Institute of Chemistry, Chinese Academy of Sciences, in 2006 under the supervision of Prof. Dao-Ben Zhu. She is currently working as a professor at the University of Chinese Academy of Sciences. Her research interests are helicene chemistry and optoelectronic functional materials.

Chuan-Feng Chen

Chuan-Feng Chen has been working as a full professor of organic chemistry at the Institute of Chemistry, Chinese Academy of Sciences, since 2001. His current research includes supramolecular chemistry based on synthetic macrocyclic hosts, stimulus responsive supramolecular materials, optoelectronic materials and devices, and helicene chemistry.

this review will provide a cohesive framework for the understanding of WCPL phenomena as well as informing the rational design of next-generation chiral luminescent materials with translational potential from fundamental research to optoelectronic applications.

2. The basic concepts and detection methods of WCPPL and WCPEL

According to different white light generation mechanisms, WCPL can be classified into white circularly polarized photoluminescence (WCPPL) and white circularly polarized electroluminescence (WCPEL). WCPPL materials primarily achieve white emission through excited-state energy transfer or the synergistic effect of multicomponent emissive systems, whereas WCPEL is based on the radiative recombination of electrically injected charge carriers within the emissive layer under electrical excitation. The chiroptical activity of these systems is quantified using dissymmetry factors, including the photoluminescence dissymmetry factor (g_{PL}) and the electroluminescence dissymmetry factor (g_{EL}), both defined analogously to the general luminescence dissymmetry factor (g_{lum}).

For WCPPL systems, the evaluation of comprehensive performance requires simultaneous consideration of chiroptical characteristics, photoluminescence performance and white-light emission quality. As previously discussed, chiroptical performance is evaluated using dissymmetry factors, which will not be reiterated here. Photoluminescence performance is primarily quantified by the photoluminescence quantum yield (PLQY), defined as the ratio of emitted photons to absorbed photons. A higher PLQY indicates more efficient radiative decay, contributing to enhanced brightness and energy efficiency in practical applications. The evaluation of white-light emission quality typically relies on three key metrics: CIE coordinates, CRI and CCT. The CIE coordinates provide a quantitative description of perceived color, with standard white light located at (0.33, 0.33). The CRI evaluates how faithfully a light source reproduces the colors of various objects compared to a reference source.[27] Generally, CRI values above 80 are typically deemed for indoor-lighting, while values above 90 are essential for high-fidelity color applications, such as photography, display technology, and medical diagnostics.[28] CCT refers to the hue of a light source, expressed as the temperature of a blackbody radiator emitting a similar spectrum. Lower CCTs (2700–3000 K) produce warm white light suitable for residential and hospitality settings, while higher CCTs (5000–6500 K) yield cool white light commonly used in offices, laboratories, and clinical environments.[29–31] Therefore, the ability to tailor CCT alongside the high CRI value, the high $|g_{lum}|$ value, high PLQY and appropriate CIE coordinates is crucial for WCPPL materials.

For WCPEL systems, the evaluation criteria are analogous to those of WCPPL systems but require additional consideration of electroluminescence properties. The electroluminescence performance is primarily assessed based on key parameters such as luminance, external quantum efficiency (EQE), efficiency roll-off, device operational lifetime and electroluminescence stability. Collectively, these metrics characterize the emission efficiency and operational stability of electrically excited materials, establishing critical indicators for assessing their viability in practical optoelectronic devices.

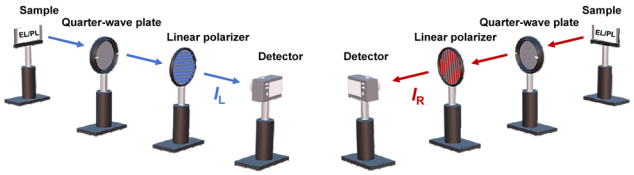

Fig. 3 Schematic illustration of the detection mechanisms for WCPPL and WCPEL.

The CPL spectra of WCPPL and WCPEL are acquired using a CPL spectrometer equipped with a dual-channel detection system incorporating a quarter-wave plate and polarizing optics (Fig. 3).[32] Crucially, this setup enables simultaneous differential detection of left- (I_L) and right-handed (I_R) circularly polarized emissions through real-time parallel measurement – an essential feature for minimizing artifacts arising from photo- or electrochemical instability of the samples. The luminescence dissymmetry factor (g_{lum}) was subsequently derived through quantitative analysis of these polarization-resolved signals. For white-emission systems, it is imperative to record CPL spectra across the entire visible range (400–700 nm) to comprehensively evaluate the spectral uniformity and wavelength dependence of the chiroptical response.

3. WCPL based on polymer materials

Given the advantages of polymer materials in solution-processability large-area fabrication, flexibility, and low-cost scalability, the development of polymer-based WCPL materials has emerged as a crucial research frontier. Based on the origin of chirality, polymer-based WCPL materials can be categorized into intrinsically chiral polymers and chirality-induced polymer systems. Furthermore, three primary strategies have been developed based on distinct white-light generation mechanisms: (i) engineering blue-emitting polymers capable of forming excimers or exciplexes (*e.g.*, *via* π–π stacking or charge-transfer interactions), where the resultant yellow/orange emission is combined with blue emission to yield white light; (ii) designing single-polymer systems with multi-chromophore segments, which enables white emission *via* intramolecular energy transfer; and (iii) blending chiral polymers with complementary emissions, wherein the spectral overlap between different components is carefully tuned to produce balanced white light. Each strategy involves distinct design considerations: the first relies on rational molecular design to achieve efficient excimer formation with well-matched emission spectra; the second demands rigorous control over polymerization processes, including the monomer ratio, sequence distribution, and molecular weight distribution; and the third requires precise control

over the ratio of individual components to achieve the desired white light emission.

3.1 WCPPL based on polymer materials

3.1.1 WCPPL based on single-polymer chain materials. A common strategy for constructing chiral polymers involves incorporating chiral units into the side chains of the polymer backbone. Following this approach, Nakano *et al.* synthesized the chiral side-chain polymer, **poly(BBPDBF)**, by terminating the polymer with chiral methyl groups (Fig. 4(a)).[21] Interestingly, this polymer exhibited a markedly different photophysical characteristic in solution and solid states (Fig. 4(b) and (c)). In dilute solution, **poly(BBPDBF)** only displayed a blue emission band. In contrast, thin films of **poly(BBPDBF)** exhibited significant spectral broadening and a dual-emission profile, indicative of the formation of excimer-like states in the solid phase. Furthermore, when the annealing duration was prolonged, the intensity of the long-wavelength emission component was markedly enhanced, which could be attributed to the thermally induced enhancement of inter-chain π–π stacking interactions (Fig. 4(c)). Besides, **poly(BBPDBF)** exhibited a distinct CPL signal in the solid-state film, with a $|g_{PL}|$ value of 6×10^{-4} (Fig. 4(d)). This study represented the first report of dual-emission white-light generation from a conjugated polymer, providing valuable insights into the rational molecular design of future white-emission chiroptical polymeric materials.

Similarly, chiral side-chain engineering has also been extended to block copolymer systems. Wu *et al.* reported a series of amphiphilic chiral copolymers, **P3HT-*b*-PPI**, comprising a π-conjugated poly(3-hexylthiophene) (**P3HT**) block and an optically active helical poly(phenyl isocyanate) (**PPI**) segment (Fig. 5).[22] These block copolymers were capable of forming well-defined cylindrical helical micelles *via* crystallization-driven asymmetric self-assembly. The resulting structures exhibited solvent-dependent photoluminescence behaviors, with

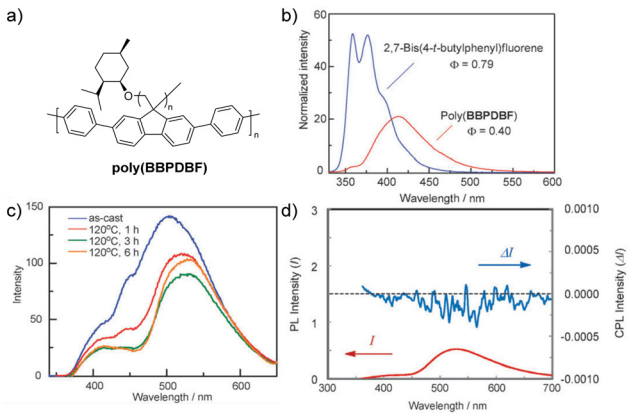

Fig. 4 (a) The molecular structure of **poly(BBPDBF)**. (b) Normalized fluorescence spectra of **poly(BBPDBF)** and 2,7-bis(4-*t*-butylphenyl)-fluorene (λ_{ex} 322 nm). (c) Fluorescence spectra of **poly(BBPDBF)** measured after thermal annealing at 120 °C (λ_{ex} 329 nm). (d) CPL spectra of **poly(BBPDBF)** annealed at 120 °C for 6 h. Reproduced with permission from ref. 21. Copyright 2011, Royal Society of Chemistry.

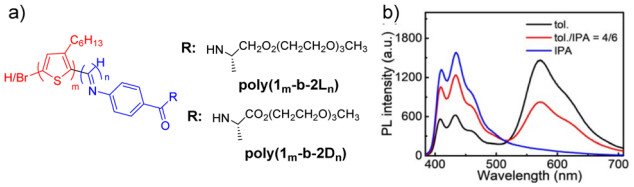

Fig. 5 (a) The molecular structure of **P3HT-*b*-PPI**. (b) Normalized fluorescence spectra of **P3HT-*b*-PPI** in different solutions. Reproduced with permission from ref. 22. Copyright 2020, Wiley-VCH.

emission color tunable from orange in toluene, to white in a mixed solvent system (toluene/isopropanol = 4 : 6, CIE coordinates: 0.32, 0.28), and to blue in pure isopropanol (Fig. 5(b)). Moreover, under excitation at 390 nm, distinct mirror-image CPL signals were observed, with a ($|g_{PL}|$) of 3.6×10^{-3}. This chiroptical activity was attributed to the formation of hierarchical chiral supramolecular assemblies facilitated by the helical **PPI** segments. This work presented a novel and effective strategy for realizing WCPPL emission through the hierarchical chiral assembly of block copolymers.

3.1.2 WCPPL based on multi-polymer doping materials. Blending chiral polymers with complementary emission characteristics offers a promising strategy for achieving WCPPL, relying on precise control over blending ratios to finely tune the red-green-blue (RGB) emission balance. In 2012, Akagi *et al.* successfully synthesized a series of novel chiral liquid-crystalline polythiophene derivatives and their phenyl copolymers by introducing chiral alkoxy carbonyl substituents into the side chains of polythiophenes (Fig. 6).[17] These polymers exhibited red, green, and blue CPL emission in the solid film, with $|g_{PL}|$ values on the order of 10^{-2}. Meaningfully, upon thermal annealing, the $|g_{PL}|$ values were enhanced, reaching the order of 10^{-1}. This was attributed to the formation of well-ordered helical π–π stacking structures during the liquid-crystalline reorganization process. Furthermore, WCPPL emission was achieved by precisely controlling the blending ratios of polymers ***S*-/*R*-P(TTT*)**, ***S*-/*R*-P(TTP*)**, and ***S*-/*R*-P(PPT*)**, with $|g_{PL}|$ values on the order of 10^{-3}. This work represented one

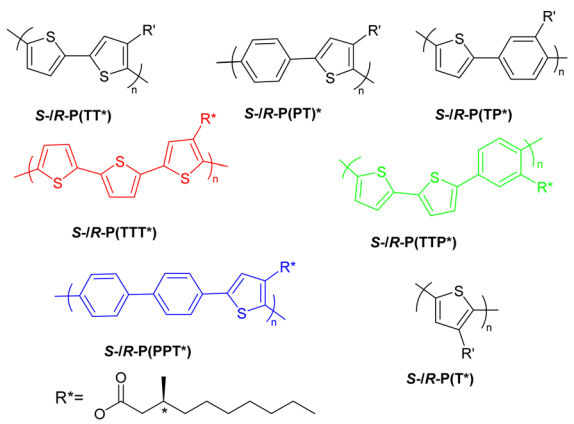

Fig. 6 The molecular structure of chiral liquid-crystalline polythiophene derivatives and their phenyl copolymers.

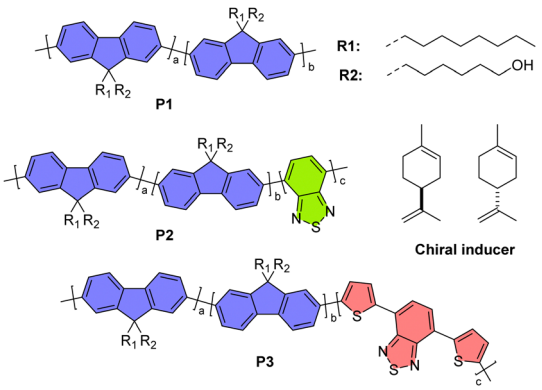

Fig. 7 The molecular structure of polymers **P1**, **P2**, **P3** and the chiral inducer.

of the earliest demonstrations of enhancing CPL dissymmetry through polymer annealing, providing valuable guidance for the development of high-performance WCPL materials.

Through the cooperative organization of chiral inducers and emissive polymers, chiral co-assembly offers an efficient route for modulating CPL signals. In 2024, Zhang *et al.* reported a novel strategy for the precise modulation of CPL signals through polymer chiral co-assembly and contactless dynamic chiral communication (Fig. 7).[33] CPL-active supramolecular co-assembly thin films with finely tunable emission colors were constructed by co-doping polymers **P1**, **P2** and **P3** with chiral inducers in carefully optimized ratios. Remarkably, ideal WCPPL films were prepared by blending **P1**, **P2** and **P3** in the ratio of 70 : 30 : 2, yielding bright white emission with CIE coordinates of (0.33, 0.33), a PLQY of 80.8% and a $|g_{PL}|$ value of 1.4×10^{-2}. Moreover, a dynamic chiral communication platform was established wherein CPL-active films interacted with chirality-selective absorption films based on PAzo

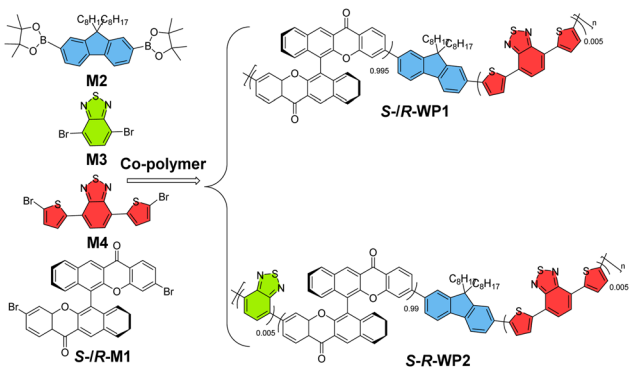

Fig. 8 The molecular structure of polymers ***S*-/*R*-WP1** and ***S*-/*R*-WP2**.

derivatives, enabling CPL signal attenuation, inversion, and amplification.

3.2 WCPEL based on polymer materials

For WCPEL systems, the design strategy must integrate foundational methodologies from photoluminescent systems while critically addressing charge carrier recombination dynamics under electrical excitation. This process typically involves the formation and modulation of electroplexes and electromers at heterojunction interfaces, which significantly influence both optical performance and electrical characteristics of the devices.[34–36] Therefore, optimizing device performance necessitates a comprehensive design framework that precisely coordinates charge injection, transport, and recombination dynamics to simultaneously achieve high efficiency, superior color fidelity, and long-term operational stability.

In 2022, Cheng *et al.* reported white circularly polarized organic light-emitting diodes (CP-WOLEDs) with chiral conjugated polymers as emitters (Fig. 8).[37] Axially chiral white-emission polymers ***S*-/*R*-WP1** were obtained through precise ternary copolymerization, incorporating blue-emitting **M2**, red-emitting **M4**, and the chiral structural unit ***S*-/*R*-M1** as the configurational backbone, which exhibited dual emission under both photo- and electroluminescence. However, incomplete spectral coverage led to a low CRI value. To further enhance the CRI value of white light, a quaternary copolymer ***S*-/*R*-WP2** was developed. This copolymer incorporates an additional green-emissive segment (**M3**), along with **M2**, **M4**, and ***S*-/*R*-M1**. It demonstrated well-balanced RGB emission characteristics, achieving a substantially enhanced CRI of 95. Furthermore, CP-WOLEDs based on ***S*-/*R*-WP2** were achieved, which exhibited WCPEL with CIE coordinates of (0.32, 0.33)/(0.33, 0.34), a CCT of 6492/6343 K, a maximum external quantum efficiency (EQE_{max}) of 0.54%/0.50%, a maximum luminance (L_{max}) of 3001/3013 cd m^{-2} and $|g_{EL}|$ values on the order of 10^{-3}. While quaternary copolymerization enabled a high CRI value, the modest $|g_{EL}|$ value reflected limited supramolecular chirality transfer, attributable to the polymer matrix's disordered microstructure. Meanwhile, CP-WOLEDs based on ***S*-/*R*-WP2** exhibited stable electroluminescence spectra at various luminance values (Table 1).

To further enhance the $|g_{EL}|$ value while maintaining the high CRI of WCPEL, this group developed high performance CP-WOLEDs based on the chiral co-assembly strategy in 2023 (Fig. 9).[12] After thermal annealing treatment, the chiral inducers (***S*-/*R*-M**) and ternary copolymers (***w*-WP** and ***c*-WP**) formed co-assembled helical nanofiber structures through intermolecular π–π interactions, leading to a significant enhancement in the $|g_{PL}|$ value (Fig. 9(b)). Furthermore, CP-WOLEDs incorpor-

Table 1 WCPEL performance based on polymer materials

Entry	Emitters	CIE coordinates	CRI	$\|g_{EL}\|$	L_{max} (cd m^{-2})	EQE_{max} (%)	Ref.
1	***S*/*R*-WP2**	(0.32, 0.33)	95	10^{-3}	3001	0.54	37
2	**(*S*-/*R*-M)$_{0.2}$-(*c*-WP)$_{0.8}$**	(0.33, 0.33)	98	0.062	11 351	1.4	12
3	***R*-/*S*-E-0.1**	(0.33, 0.51)	75	2.4×10^{-3}	3919	15.1	39

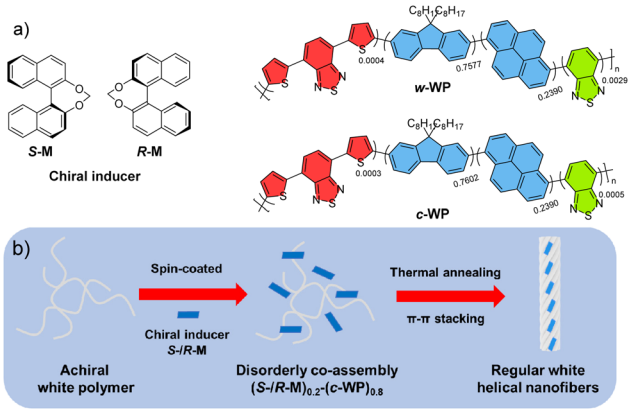

Fig. 9 (a) The molecular structure of polymers ***w*-WP** and ***c*-WP** and the chiral inducer. (b) Schematic illustration of the chiral co-assembly WCPEL route.

ating these co-assemblies as emitters were successfully fabricated. The optimized devices exhibited ideal white-light emission with CIE coordinates of (0.33, 0.33), a CRI of 98, a CCT of 5725 K, a $|g_{EL}|$ value of 0.062, an EQE_{max} of 1.4%, and an L_{max} of 11 351 cd m^{-2}. Furthermore, the CP-WOLED devices with **(*S*-/*R*-M)$_{0.2}$-(*c*-WP)$_{0.8}$** as emitters exhibited good color stability at different operating voltages. This study provided an effective approach for amplifying the $|g_{EL}|$ value of WCPEL. However, the device still suffered from a relatively low EQE_{max}, which is primarily attributed to the intrinsic limitation of the internal quantum efficiency (IQE) of conventional fluorescent emitters, capped at 25%.[38]

WCPEL can alternatively be realized through electroplex formation at donor–acceptor heterojunctions, where interfacial charge transfer states enable broad-spectrum emission with chiral characteristics. In 2024, Wang *et al.* reported the fabrication of CP-WOLEDs based on the strategy of electroplex emission (Fig. 10).[39] Chiral TADF polymers ***R*-/*S*-E-0.1** were synthesized *via* random copolymerization of chiral chromophores with styrene units. Furthermore, single-emissive-layer devices were fabricated utilizing chiral polymers ***R*-/*S*-E-0.1** as the sole emitters, with 1,1-bis[(di-4-tolylamino)phenyl]-cyclohexane (TAPC) serving as the host material in a single-dopant architecture. This device exhibited white emission with an EQE_{max} of 15.1%, CIE coordinates of (0.33, 0.51), a $|g_{EL}|$ of 2.4×10^{-3}, a CRI of 75, and an L_{max} of 3919 cd m^{-2}. This study

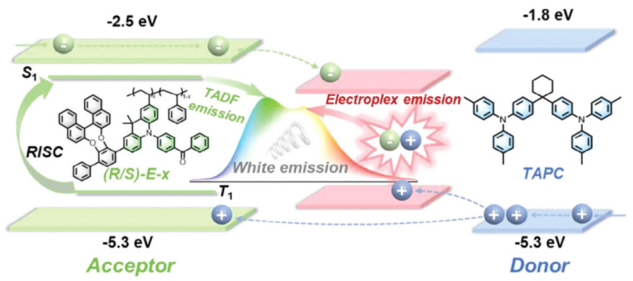

Fig. 10 Schematic illustration of the white electroplex emission mechanism found between chiral polymers ***R*-/*S*-E-*x*** and TAPC. Reproduced with permission from ref. 39. Copyright 2025, Wiley-VCH.

represented the first successful implementation of the single-emissive-layer exciton–electroplex hybrid emission strategy for solution-processed CP-WOLEDs, demonstrating a novel approach to CP-WOLED fabrication.

4. WCPL based on multi-component materials

Compared to polymer-based WCPL systems, the use of WCPL systems based on multicomponent emitters currently represents the most widely adopted approach. Currently, two primary approaches were employed to realize WCPL in multi-component materials: (i) precise blending of two or three chiral luminophores with complementary emission characteristics, leveraging the synergistic interplay of their intrinsic chiroptical properties to achieve broad-spectrum WCPL coverage, and (ii) controlled mixing of two or three non-chiral emissive guests exhibiting complementary luminescent colors, followed by the incorporation of chiral dopants (*e.g.*, chiral small molecules or chiral ligands), thereby imparting CPL activity to the system through the chirality induction mechanism. In both strategies, the relative ratios of emitters need to be precisely controlled to guarantee balanced emission intensities of RGB and attain the desired white-light CIE coordinates. Moreover, the concentration of the chiral dopant should be optimized to maximize the $|g_{lum}|$ value while sustaining high PLQY.

To further increase the $|g_{lum}|$ value of the WCPL system, various strategies, such as supramolecular assembly, host–guest interactions, and chiral ligand engineering, have been widely employed. These approaches will be discussed in detail in the following sections.

4.1 WCPPL based on multi-component materials

4.1.1 WCPPL based on multi-component organic–inorganic hybrid materials

4.1.1.1 WCPPL based on multi-component chirality-induced organic–inorganic hybrid materials. Organic–inorganic hybrid systems offer a versatile platform for constructing CPL-active materials, enabling efficient chirality transfer from organic chiral sources to achiral inorganic emitters *via* controlled molecular interactions. In 2017, Liu *et al.* achieved full-color and white CPL systems through the supramolecular self-assembly of achiral quantum dots (QDs) with chiral gelators (Fig. 11).[19] Full-color co-gels comprising achiral QDs and chiral

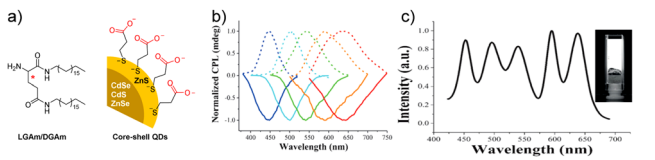

Fig. 11 (a) The structure of gelators **LGAm/DGAm** and QDs. (b) CPL spectra of full-color co-gels (λ_{ex} 360 nm). (c) Fluorescence spectra of the white-emission co-gel. Inset: Photograph of the white-emission gel under UV irradiation. Reproduced with permission from ref. 19. Copyright 2017, Wiley-VCH.

gelators (**LGAm/DGAm**) were assembled *via* electrostatic interactions between QD-surface carboxylates and gelator amines (Fig. 11(a) and (b)). By optimizing the doping ratios of five distinct colored QDs to 4 : 2 : 3 : 3 : 3 (blue/cyan/green/yellow/red) within the gel matrix, the first white-emission QDs were successfully developed, exhibiting WCPPL characteristics with CIE coordinates of (0.33, 0.35) and a $|g_{PL}|$ of 5×10^{-4} (Fig. 11(c)). While no significant CPL signal was observed in a simple solution mixture of QDs and chiral inducers, the co-gel system exhibited remarkable chiroptical activity. This finding confirmed the critical role of supramolecular gelation in facilitating efficient chirality transfer.

Beyond transfer from chiral organic molecules to inorganic emissive components, the encapsulation of achiral fluorescent dyes within chiral metal–organic frameworks (CMOFs) was also a widely adopted strategy for constructing full-color and white CPL-active systems *via* confinement-induced chirality transfer. In 2020, Zang *et al.* reported a series of full-color CPL-active crystalline composite materials by *in situ* encapsulation of multiple achiral fluorescent dyes – such as **CBS** (blue), **FS** (green), **Rhodamine B** (**RhB**, red), **R6G** (orange) and **AR** (light red) – within nanoscale helical channels of CMOFs (Fig. 12(a) and (b)).[40] The chiral host frameworks, available as enantiomeric L-/D-forms, enabled non-covalent immobilization of the dyes *via* hydrogen bonding within the chiral pores. This confinement induced chirality transfer from CMOF scaffolds to the encapsulated achiral dyes, resulting in CPL from achiral fluorophores. Notably, by co-encapsulating **CBS**, **FS**, and **RhB** in an optimized ratio within **L-/D-CMOFs** (denoted as **L-/D-CMOF ⊃ CBS/FS/RB**), white-light CMOFs were achieved with CIE coordinates of (0.33, 0.32), a PLQY of 30%, and a $|g_{PL}|$ value on the order of 10^{-3}. Furthermore, white light-emitting diode (WLED) devices were fabricated by coating **L-/D-CMOF ⊃ CBS/FS/RB** films onto UV-LEDs, which exhibited bright white-light CPL. This study offered a versatile strategy for constructing full-color and white-light CPL-active materials.

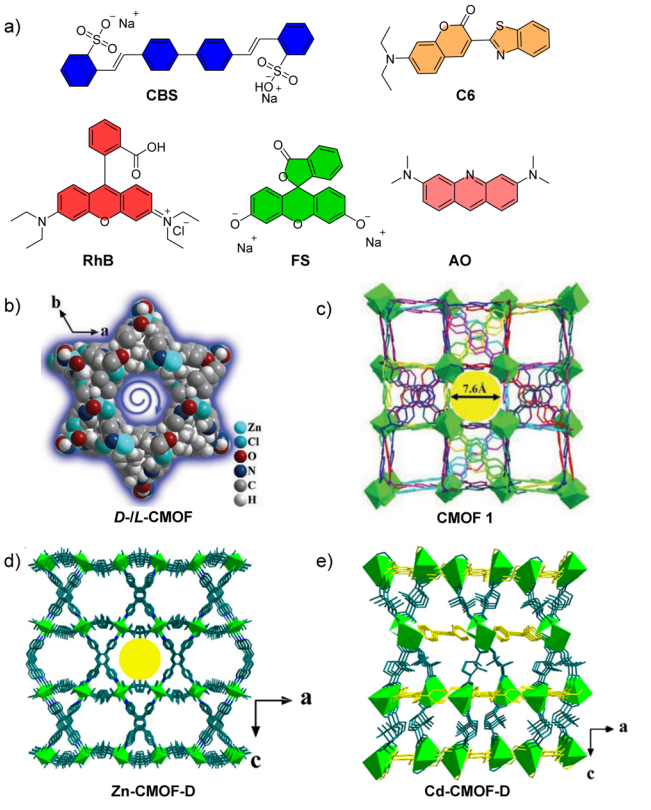

Fig. 12 (a) The molecular structure of achiral dyes **CBS**, **RhB**, **FS**, **AO** and **C6**. (b) The 3D framework **D/L-CMOF** with helical channels. (c) The 3D eightfold interpenetrated framework of CMOF **1**. (d) The 3D framework of **Zn-CMOF-D** and (e) **Cd-CMOF-D**. Reproduced with permission from ref. 40. Copyright 2020, Wiley-VCH. Reproduced with permission from ref. 14. Copyright 2020, Wiley-VCH. Reproduced with permission from ref. 41. Copyright 2022, American Chemical Society.

In the same year, Du *et al.* synthesized porous CMOF **1**, employing tris[4-(4′-carboxyl)biphenyl]amine (**TCPA**) as a linker and Cd^{2+} centers as a metal node (Fig. 12(c)).[14] CMOF **1** not only exhibited room-temperature phosphorescence (RTP) properties but also demonstrated excellent optical anisotropy. Furthermore, CMOF ⊃ dye host–guest systems were constructed utilizing CMOF **1** as the host and various fluorescent dyes (*e.g.*, **Coumarin 6** (**C6**) and **RhB**) as guests, which exhibited multicolor RTP-fluorescence dual emission. Notably, through optimizing the ratio of **RhB** and host materials, the white-emission host–guest system of CMOF **1 ⊃ RhB** was obtained with CIE coordinates of (0.33, 0.33).

In 2022, Li *et al.* constructed two pairs of CMOFs, **Zn-CMOF-D/L** and **Cd-CMOF-D/L**, through the self-assembly of D-/L-camphoric acid (**D-/L-cam**) and an achiral fluorescent ligand, 1,2,4,5-tetra(pyridin-4-yl)benzene, with Cd^{2+} and Zn^{2+} ions (Fig. 12(d) and (e)).[41] Notably, **Cd-CMOF-D** and **Cd-CMOF-L** exhibited strong intrinsic CPL activity with $|g_{PL}|$ values of 0.010 and 0.009, respectively. This can be attributed to their high porosity and rigid frameworks, which enhance chiral exciton coupling and suppress non-radiative decay. To further achieve tunable emission across the visible spectrum, organic dyes including **C6** and Acridine Orange (**AO**) were encapsulated into **Zn-CMOF** pores, forming host–guest systems capable of generating emission from blue to white (Fig. 12(a)). The white-emitting **Zn-CMOF ⊃ AO** composite was coated onto UV-LED chips to fabricate white LED devices which exhibited bright white-light emission with CIE coordinates of (0.34, 0.33), a CCT of 4886 K, and a high CRI of 91.

4.1.1.2 WCPPL based on multi-component intrinsically chiral organic–inorganic hybrid materials. In 2021, Hisaeda *et al.* developed trivalent aluminum-based dinuclear triple-stranded helicate **ALPHY** *via* a simple two-step synthesis method (Fig. 13).[25] These complexes showed multicolor (cyan, yellow, and orange) photoluminescence. Through asymmetric resolution, optically pure right-handed (*P*) and left-handed (*M*) enantiomers were successfully isolated, exhibiting CPL with $|g_{PL}|$ values on the order of 10^{-3}. White photoluminescence with CIE coordinates of (0.28, 0.34) was achieved through controlled stoichiometric blending of the cyan-emitting (**1**) and yellow-emitting (**2**) components at an optimized 7 : 3 molar ratio. This work provided a novel

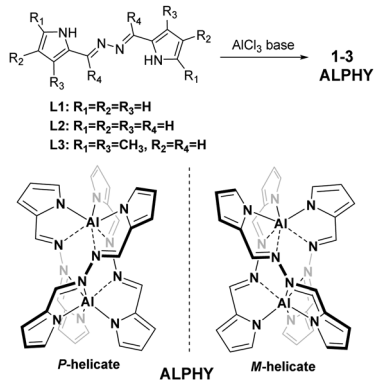

Fig. 13 Synthesis scheme and stereochemical representations of **ALPHY 1-3**: (*P*)- and (*M*)-helical enantiomers.

approach for designing multifunctional chiral optical materials, although the achieved $|g_{PL}|$ values remain relatively low for practical applications.

In 2024, Zhao *et al.* successfully designed and synthesized highly stable chiral five-coordinate manganese(II) complex ***R*-/*S*-[(L$_2$)MnBr]Br** incorporating phosphine oxide ligands (Fig. 14(a) and (b)).[42] Both ***R*-[(L$_2$)MnBr]Br** and ***S*-[(L$_2$)MnBr]Br** exhibited bright red photoluminescence and outstanding CPL characteristics with g_{PL} values of $+1.56 \times 10^{-2}$ and -1.94×10^{-2}, respectively. Furthermore, white-emission films were prepared by mixing ***S*-[(L$_2$)MnBr]Br** with commercially available blue phosphor **BaMgAl$_{10}$O$_{17}$:Eu^{2+}** and green phosphor **(Ba,Sr)$_2$SiO$_4$:Eu^{2+}** in an optimized ratio and coating the mixture onto a UV LED chip. The LED device exhibited warm white-light emission, with CIE coordinates of (0.36, 0.38), a CCT of 4512 K, and an exceptionally high CRI of 96.9 (Fig. 14(b)). This study provided valuable insights into the development of multifunctional chiral manganese(II)-based luminescent materials.

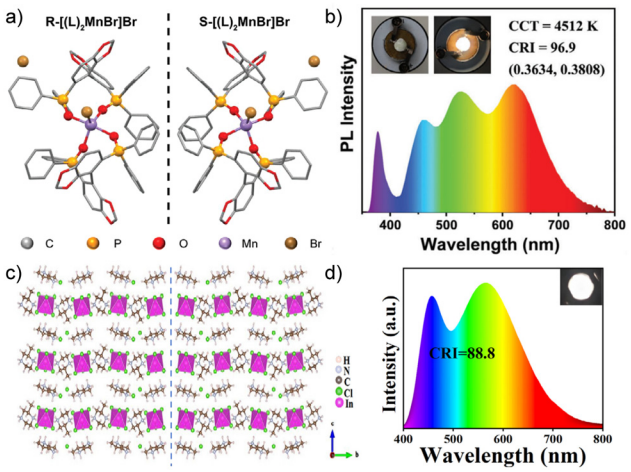

Fig. 14 (a) Crystal structures of ***R*-[(L$_2$)MnBr]Br** (left) and ***S*-[(L$_2$)MnBr]Br** (right). (b) The emission spectra of white LEDs based on ***S*-[(L$_2$)MnBr]Br**. (c) Packing structures of **R_2InCl$_7$** (left) and **S_2InCl$_7$** (right). (d) The emission spectra of white LEDs based on **S-(R/S)$_2$InCl$_7$**. Reproduced with permission from ref. 42. Copyright 2024, Wiley-VCH. Reproduced with permission from ref. 43. Copyright 2025, Wiley-VCH.

Recently, Zou *et al.* reported chiral hybrid metal chloride materials with multi-modal dynamic responsiveness, demonstrating their applications in LEDs (Fig. 14(c) and (d)).[43] Under photoexcitation, Sb^{3+}-doped **(*R*/*S*)$_2$InCl$_7$** exhibited highly efficient broadband yellow CPL emission with the PLQY approaching 100% and a $|g_{PL}|$ value of 1.7×10^{-3}. Interestingly, exposure to a humid environment triggered a structural transformation in Sb^{3+}-doped **(*R*/*S*)$_2$InCl$_7$**, resulting in the formation of a non-emissive hydrated phase, Sb^{3+}-doped **(*R*/*S*)$_2$InCl$_7$·H$_2$O**. In addition, Sb^{3+}-doped **(*R*/*S*)$_2$InCl$_7$** exhibited a unique nonlinear optical response, enabling reversible switching between yellow emission and non-emission by adjusting the rotation angle between the quarter-wave plate and the linear polarizer. Leveraging these unique photophysical properties, white-emission films were obtained by mixing commercial blue phosphor **BaMgAl$_{10}$O$_{17}$:Eu^{2+}** with Sb^{3+}-doped **(*R*/*S*)$_2$InCl$_7$** in an optimized ratio followed by deposition onto a UV LED chip. The resulting LED device exhibited white-emission with a CRI of 88.8 and a $|g_{PL}|$ value of 1.67×10^{-3}. Furthermore, by adjusting the rotation angle of the linear polarizer, tunable white light emission was achieved, enabling transition from warm white to neutral white (Fig. 14(d)). Correspondingly, the CIE coordinates shifted from (0.39, 0.43) to (0.32, 0.35), with the CCT varying from 4000 K to 6000 K.

4.1.2 WCPPL based on multi-component purely organic materials. Compared with organic–inorganic hybrid materials, purely organic luminescent materials offered broader raw material sources and lower synthesis costs, thereby offering greater potential for scalable and cost-effective production. In the following sections, we summarize recent advances in WCPPL achieved through purely organic multi-component emissive systems.

4.1.2.1 WCPPL based on multi-component intrinsically chiral purely organic materials. In 2018, our group reported a series of organic nanoparticles formed *via* the self-assembly of spirochiral aromatic amide enantiomers ***P*-/*M*-1a-e**, which exhibited tunable full-color photoluminescence and high PLQYs (Fig. 15(a) and (b)).[20] By Förster resonance energy transfer

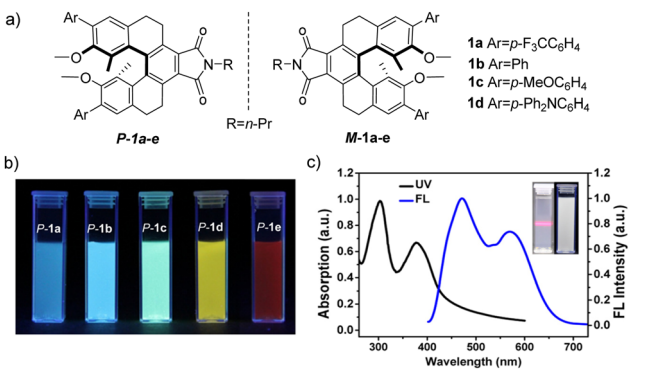

Fig. 15 (a) The molecular structure of full-color chiral dyes **1a–1d**. (b) Dispersion colors of full-color chiral nanoparticles ***P*-1a-e** (λ_{ex} 365 nm). (c) The UV-VIS and fluorescence emission spectra of white-emission nanoparticles. Reproduced with permission from ref. 20. Copyright 2018, American Chemical Society.

(FRET) among three primary-color emissive enantiomers-***M*-1a** (blue), ***M*-1d** (green), and ***M*-1e** (red), WCPPL chiral organic nanoparticles were successfully fabricated. These nanoparticles exhibited WCPPL with CIE coordinates of (0.30, 0.33) and $|g_{PL}|$ values on the order of 10^{-3} (Fig. 15(c)). This study represented the first successful fabrication of full-color and white chiral organic nanoparticle materials.

In 2021, Lu *et al.* reported the synthesis of full-color and white CPL-active multicolor chiral carbonized polymer dots (Ch-CPDs) (Fig. 16).[44] Multicolor Ch-CPDs with tunable emission ranging from blue to red were synthesized *via* a solvothermal approach at a fixed temperature, using L-/D-tryptophan (**L-/D-Trp**) and *o*-phenylenediamine as molecular precursors. Meanwhile, mirror-image CD spectra of B-/Y-/R-L-CPDs and B-/Y-/R-D-CPDs were observed. Furthermore, multicolor Ch-CPDs were incorporated into organic lipid gels (**DGAm/LGAm**) *via* supramolecular self-assembly, leading to the generation of tunable CPL properties. By precisely adjusting the ratios of blue-, yellow-, and red-emitting Ch-CPDs, the white CPL-active Ch-CPD co-gel system was successfully fabricated for the first time, exhibiting CIE coordinates of (0.30, 0.33) and a $|g_{PL}|$ value of 2.5×10^{-3}. This work presented a simple and controllable synthetic approach to obtain full-color and white-emitting Ch-CPDs, offering a new strategy for designing chiral carbon-based materials with superior optical properties.

4.1.2.2 WCPPL based on multi-component chirality-induced purely organic materials. In contrast to intrinsically chiral luminophores, chiral induction strategies provide an efficient and versatile pathway for achieving full-color and white CPL, without the need for elaborate molecular design. Chiral induction strategies rely on the transfer of chiral information from external chiral sources – such as enantiopure small molecules,

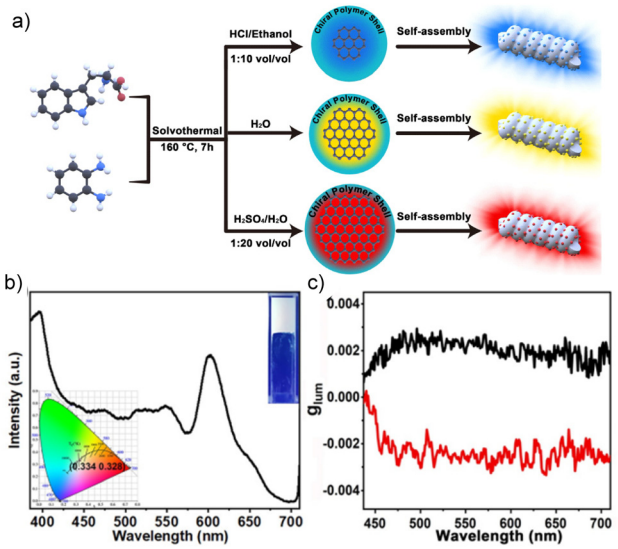

Fig. 16 (a) Schematic illustration of the synthetic procedure for multicolor-emissive chiral carbonized polymer dots (Ch-CPDs). (b) PL spectra of the white-emission cogel (λ_{ex} 365 nm). (c) The g_{lum} *versus* wavelength of DGAm/L-CPDs (black) and LGAm/D-CPDs (red). Reproduced with permission from ref. 44. Copyright 2021, Wiley-VCH.

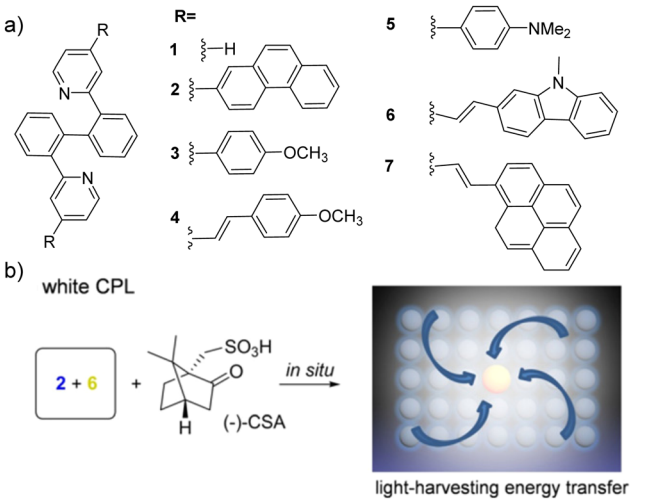

Fig. 17 (a) The molecular structure of pyridine derivatives **1–7**. (b) WCPL microcrystals. Reproduced with permission from ref. 26. Copyright 2021, Wiley-VCH.

chiral polymers, or supramolecular frameworks – to achiral emissive components *via* non-covalent interactions, including hydrogen bonding, π–π stacking, and electrostatic forces. This process often leads to the formation of helical or asymmetrical supramolecular architectures that exhibit significant CPL activity. In recent years, this strategy has emerged as a widely adopted method for the construction of full-color and white CPL-active materials.

Among the various chiral induction strategies, the use of enantiopure small molecules as chiral inducers has emerged as one of the most commonly adopted and effective strategies. In 2018, Zhong *et al.* reported a series of CPL-active organic ionic microcrystals exhibiting both full-color and white-light emission, in which supramolecular chirality was induced *via* hydrogen-bonding interactions with enantiopure camphorsulfonic acid (**CSA**) (Fig. 17).[26] These microcrystals were prepared by reacting a series of pyridine derivatives (**1–7**) with **CSA**, achieving $|g_{PL}|$ values up to 10^{-2} and PLQYs as high as 80%. Moreover, by implementing the light-harvesting FRET mechanism, white-emission chiral microcrystals were obtained by co-assembling blue-emissive compound **2** and yellow-emissive compound **6** with **CSA** in a finely tuned molar ratio. The resulting microcrystals displayed white CPL with CIE coordinates of (0.30, 0.33), a $|g_{PL}|$ value of 0.026, and a PLQY of 46%. This work highlighted the potential of **CSA**-mediated hydrogen-bonded assemblies for creating efficient WCPL-active materials from structurally simple achiral building blocks.

Building on this concept, Feng *et al.* developed a chiral co-assembly strategy to fabricate CPL-active nanofibrous gels with tunable emission colors, including white-light emission (Fig. 18).[45] Specifically, enantiopure phenylalanine-derived gels (**LPF** and **DPF**) were co-assembled with achiral fluorophores such as 1-aminopyrene (**Py**), 2-aminoanthracene (**2-An**), 1-aminoanthracene (**1-An**), and **RhB**. Structural characterization using Fourier-transform infrared spectroscopy (FTIR) and X-ray

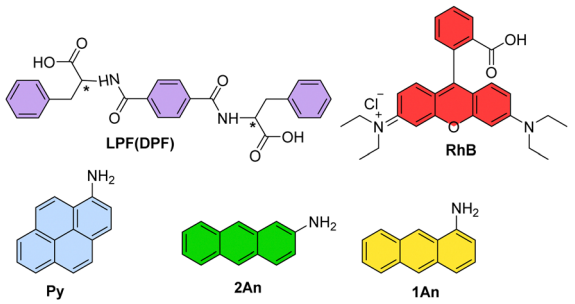

Fig. 18 The molecular structure of chiral inducer **LPF** (**DPF**) and dyes **Py**, **RhB**, **2An** and **1An**.

powder diffraction (XRD) confirmed the formation of ordered supramolecular nanofibers stabilized by π–π stacking and hydrogen bonding interactions. This hierarchical assembly facilitated the efficient transfer of chiral information from the gel to the achiral dyes, generating CPL-active materials across the visible spectrum. Furthermore, by co-assembling **Py** (blue), **2-An** (green), and **RhB** (red) in optimized proportions, white CPL-active gels were achieved, exhibiting CIE coordinates of (0.31, 0.33).

Benefiting from the inherent configurational chirality of polymers and their ability to form ordered supramolecular structures, polymer-mediated chiral induction has emerged as a robust strategy for the development of CPL-active materials. In 2022, Deng *et al.* reported the fabrication of multicolor and white nanofibers *via* electrospinning, in which chiral induction was achieved through the incorporation of a helical chiral polymer as the chiral source.[46] Multi-color CPL-active nanofibers were prepared by doping the chiral helical polymer, poly[(*S*)-3,3′-diisocyanato-2,2′-binaphthyl-*co*-1,4-phenylene] (**PSA**), along with various achiral fluorescent dyes – **ACA** (blue), **BPA** (green), **Rh6G** (yellow), **RhB** (red), and **Nile Red** (**NR**, red) – into the polyacrylonitrile (**PAN**) matrix (Fig. 19). Furthermore, white-emission nanofibers were achieved by blending **ACA** and **Rh6G** in optimized ratios during uniaxial electrospinning, yielding white emission with CIE coordinates of (0.30, 0.34). To enhance uniformity, coaxial electrospinning was employed to spatially separate dyes into core–shell structures, resulting in white CPL nanofibers with CIE coordinates of (0.32, 0.33), a PLQY of 36.0%, and a $|g_{PL}|$ value of 4.0×10^{-3}. These nanofiber films were further coated onto UV chips, demonstrating bright white emission with CIE coordinates of (0.32, 0.33), a CRI of 31.1 and a CCT of 6362 K.

In the same year, this group introduced a distinct approach to achieving full-color and white CPL emission *via* chiral induction and regulation in polyacetylene derivatives.[47] By using chiral polylactic acid (**PLA**) as a chiral inducer, achiral polymer **P1** was induced to adopt a single-handed helical conformation during film formation through hydrogen bonding (Fig. 19). Subsequent incorporation of achiral fluorophores – **NR** (red), **X18** (green), and **TPE** (blue) – into the **PLA**/**P1** matrix afforded CPL-active films with distinct RGB emissions and $|g_{PL}|$ values on the order of 10^{-3} (Fig. 19). Notably, white CPL films

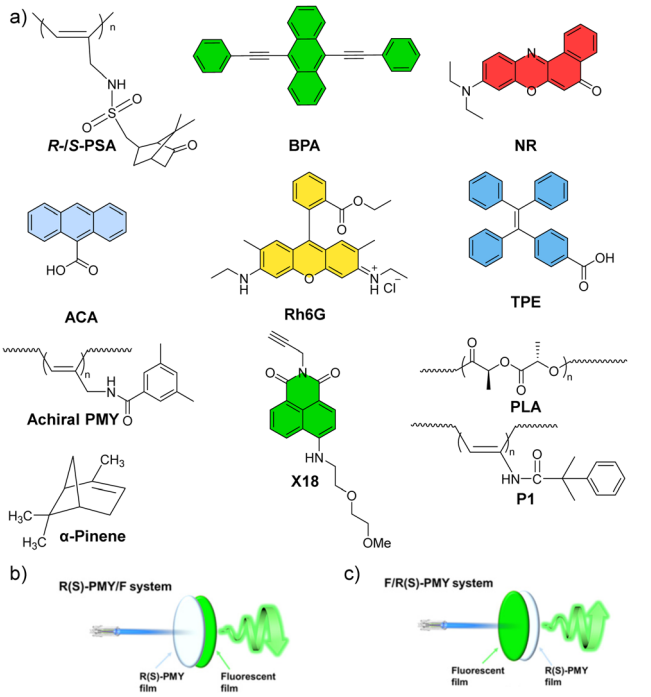

Fig. 19 (a) The molecular structures of the chiral inducers (***R*-/*S*-PSA**, **PLA**, and **α-pinene**), achiral dyes (**BPA**, **NR**, **ACA**, **Rh6G**, **TPE** and **X18**), and achiral polymers (**PMY** and **P1**). Schematic illustration of the CPL test for (b) ***R*(*S*)-PMY/F** and (c) **F/*R*(*S*)-PMY** dual-layered films. Reproduced with permission from ref. 48. Copyright 2023, American Chemical Society.

were obtained by fine-tuning the emission balance among the three fluorophores (**NR**, **X18** and **TPE**), resulting in white emission with CIE coordinates of (0.36, 0.34) and a $|g_{PL}|$ value of 4.5×10^{-3}. These films were further integrated onto UV chips, achieving full-color and white light with a CRI of 73, underscoring their potential for chiral optoelectronic applications.

To elucidate the mechanism of CPL generation, this group prepared full-color and white CPL materials *via* chirality induction and circularly polarized excitation (CP-Ex) mechanisms.[48] Helically structured polyacetylene (**PMY**) films with supramolecular chirality were constructed through π–π stacking interactions between the achiral polymer and chiral **α-pinene**. Subsequently, a series of fluorescent dyes with distinct emission – **TPE** (blue), **X18** (green), **Rh6G** (orange) and **NR** (red) – were doped into the **α-pinene**/**PMY** matrix. The resulting films displayed full-color CPL with $|g_{PL}|$ values on the order of 10^{-2}. Furthermore, the mechanism underlying CPL generation was systematically investigated using bilayer films comprising spatially separated chiral and emissive layers. When the chiral layer (***R*(*S*)-PMY**) was placed in front of the emissive layer (denoted as ***R*(*S*)-PMY/F**), the CPL response matched that of the doped system, confirming the CP-Ex mechanism. In contrast, reversing the layer order (**F/*R*(*S*)-PMY**) led to CPL signals of opposite sign, suggesting a chirality-matching mechanism (Fig. 19(b) and (c)). Importantly, by co-doping **NR**, **TPE** and **X18** into the **α-pinene**/**PMY** mixture in appropriate proportions, WCPPL films were successfully fabricated, which exhibited

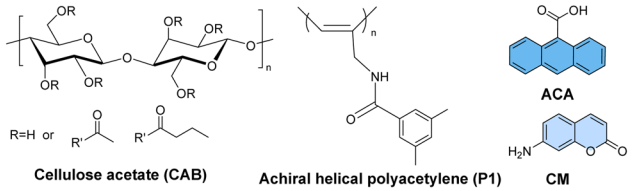

Fig. 20 The molecular structures of achiral dyes (**CM** and **ACA**), chiral inducer **CAB** and achiral polymer **P1**.

white emission with CIE coordinates of (0.31, 0.33) and a $|g_{PL}|$ value of 8×10^{-2}. This work introduced a versatile and tunable platform for constructing multicolor and white CPL materials, offering new design principles for advanced chiroptical systems.

Recently, this group also realized the amplification of configurational to conformational chirality using cellulose derivatives as chiral inducers (Fig. 20).[49] The helical structure of polyacetylene derivative **P1** was induced during film formation, primarily driven by hydrogen bonding between chiral inducers **CAB** and **P1**, with the efficiency influenced by the hydrogen-bond-accepting ability of the solvent. Furthermore, full-color CPL films were prepared by doping the **CAB/P1** matrix with four achiral dyes – **CM** (blue), **BPA** (green), **R6G** (orange), and **NR** (red) (Fig. 19 and 20). Besides, white-emission films were achieved by co-doping **ACA** and **R6G** at an optimized ratio, showing CIE coordinates of (0.33, 0.35) and a $|g_{PL}|$ of 1.6×10^{-2}. To demonstrate practical applicability, the white-light-emitting film was coated onto the UV chip to fabricate WLED devices, which displayed bright white emission.

In addition to the use of chiral small molecules and chiral polymers, chiral solvents have also been exploited to induce supramolecular chirality within luminescent systems. In 2023, Liu *et al.* reported full-color and white CPL-active liquid materials using chiral deep eutectic solvents (DESs) as a functional medium (Fig. 21).[50] The DES was formulated by combining lauric acid (hydrogen bond donor) with chiral menthol (hydrogen bond acceptor). When doped with achiral fluorophores – **CBS** (blue), **BCH** (green), **DAPI** (yellow), and **RhB** (red) – the resulting chiral DES matrix exhibited full-spectral CPL, with the handedness of CPL emissions governed by the enantiomeric configuration of menthol. Furthermore, by precisely co-doping

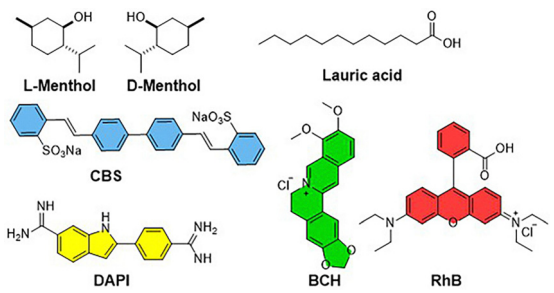

Fig. 21 The molecular structures of the chiral inducer **Menthol, Lauric acid** and achiral dyes (**DAPI**, **CBS, BCH** and **RhB**).

CBS, **BCH**, and **RhB** in the DES system, white CPL emission was achieved with CIE coordinates of (0.31, 0.32).

4.1.2.3 WCPPL based on liquid crystalline co-assembly of purely organic materials. The incorporation of chiral dopants into a nematic liquid crystal represents a classical example of chiral induction, wherein the dopants impart a helical twist to the nematic director, leading to the formation of chiral nematic liquid crystals (N*-LCs), also known as cholesteric liquid crystals (CLCs).[51] Unlike conventional chirality transfer in molecular or supramolecular systems, this process relies on long-range orientational interactions between the chiral dopants and the nematic host. Such coupling facilitates the emergence of macroscopic helical superstructures with tunable pitch lengths, often accompanied by pronounced optical activity.[52,53]

In 2021, Cheng *et al.* successfully prepared full-color N*-LCs by doping intrinsic point chiral fluorescent molecules **1a-2c** into nematic liquid crystal **E7** (Fig. 22).[18] Within the N*-LC matrix, the chiral dyes aligned into well-ordered helical superstructures, inducing pronounced chiral amplification and affording materials with markedly enhanced $|g_{PL}|$ values. Subsequently, a blue-red dual-emission strategy was employed to prepare white-emission N*-LCs, namely, **N*-LC-W1** and **N*-LC-W2**. **N*-LC-W1** was prepared by co-doping blue-emission chiral luminophore ***S*-1a** and red-emission chiral luminophore ***S*-1c** (along with their enantiomers ***R*-1a** and ***R*-1c**) into nematic liquid crystal **E7** in optimized ratios. In contrast, **N*-LC-W2** was obtained by co-doping ***S*-1a** with the enantiomeric red-emission luminophore ***R*-2c** (and correspondingly, ***R*-1a** with ***S*-2c**) into **E7** under similar optimization conditions. **N*-LC-W1** and **N*-LC-W2** exhibited white emission with CIE coordinates of (0.30, 0.34) and (0.31, 0.33), PLQYs of 34.5% and 27.6%, and $|g_{PL}|$ values reaching 0.48 and 0.46, respectively. Notably, both **S-N*-LC-W1** and **S-N*-LC-W2** systems, irrespective of whether doped with ***S*-1a**/***S*-1c** or ***S*-1a**/***R*-2c**, displayed uniformly positive CPL signals across the entire spectral range (Fig. 22(b) and (c)). This phenomenon holds significant implications for understanding the correlation between the molecular chirality and macroscopic optical activity. However, the study did not

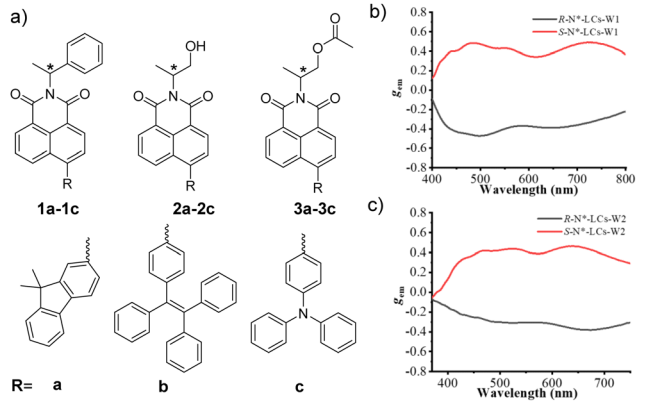

Fig. 22 (a) The molecular structures of full-color chiral dyes **1a-3c**. (b) g_{lum} values *versus* wavelength curves of **N*-LC-W1** and **N*-LC-W2**. Reproduced with permission from ref. 18. Copyright 2021, Wiley-VCH.

provide an in-depth discussion on the underlying mechanism of CPL generation in relation to chiral characteristics or the structure–property relationship between the molecular configuration and optical performance. Nevertheless, through an innovative strategy of doping chiral small molecules into nematic liquid crystals, this research successfully achieved the development of full-color and white CPL materials with high $|g_{PL}|$ values, offering new insights and technical references for the design and fabrication of chiral optoelectronic functional materials.

In 2023, Zheng *et al.* also achieved full-color and white N*-LCs by doping intrinsically chiral tetraphenylethylene derivatives ***M*/*P*-TPEH** and achiral dyes into nematic liquid crystal **5CB** (Fig. 23).[54] Their findings revealed that ***M*-TPEH** molecules induce right-handed helical stacking, thereby driving the self-assembly of the nematic liquid crystal layers into the right-handed liquid crystalline phase (*P*-LC), whereas ***P*-TPEH** promotes the formation of the left-handed liquid crystalline phase (*M*-LC). This chirality inducer mechanism significantly enhances the CPL intensity of **TPEH**, yielding $|g_{PL}|$ values of up to 0.21. Furthermore, this chirality inducer strategy can be extended to other achiral fluorescent dyes **3–6**, enabling full-color CPL emission ranging from violet to near-infrared wavelengths. By incorporating different fluorescent dyes **3-4-5-6** and chiral **TPEH** into nematic liquid crystal **5CB**, white N*-LC ***M*/*P*-1-3-4-5-6-5CB** was achieved, with CIE coordinates of (0.33, 0.33), a PLQY of 69%, and a $|g_{PL}|$ value of 0.065. Interestingly, in the mixed system of **TPEH** and achiral fluorescent dyes, the CPL signal exhibited wavelength-dependent differences in the polarization direction between **TPEH** and the fluorescent dyes (Fig. 23(b) and (c)). This intriguing phenomenon suggested the presence of complex chiral transfer and interaction mechanisms. However, the underlying causes were not thoroughly investigated by the authors, leaving room for further exploration.

Although the previous reports have enhanced the $|g_{PL}|$ value of CPL through the co-assembly of liquid crystals, the resulting $|g_{PL}|$ generally remained below 1. To further boost CPL performance, Deng *et al.* developed full-color and white CLCs with significantly enhanced $|g_{PL}|$ values by a three-level chirality transfer and amplification strategy (Fig. 24).[55] To realize full-color CPL emission, a three-component system was developed by co-assembling the chiral non-fluorescent polymer **P46** and a series of achiral fluorophores – including **ACA** (blue), **BPA** (green), **Rh6G** (yellow), and **NR** (red) – within the nematic liquid crystal **5CB**. Due to the helical supramolecular self-assembly and the Bragg reflection mechanism of CLCs, these materials exhibited intense CPL signals. Notably, WCPL CLCs were successfully achieved by precisely tuning the doping concentration of **P46** and the ratio of **ACA** to **NR**. The resulting materials exhibited white emission with CIE coordinates of (0.32, 0.33) and a high $|g_{PL}|$ value reaching 1.46. Furthermore, electrically tunable WCPL switches based on CLCs were developed, demonstrating promising potential for applications in information encryption, anti-counterfeiting technologies, and chiral logic gate systems. This study presented an effective approach for realizing high-efficiency WCPL materials, providing theoretical foundation for their practical applications.

To further enhance the $|g_{lum}|$ value of CPL in solution systems, our group recently demonstrated a strategy for CPL amplification by placing N*-LC layers behind the luminescent solution (Fig. 25).[56] For an unpolarized light with a wavelength matching the photonic bandgap of N*-LCs, the system effectively converts unpolarized light into circularly polarized light.

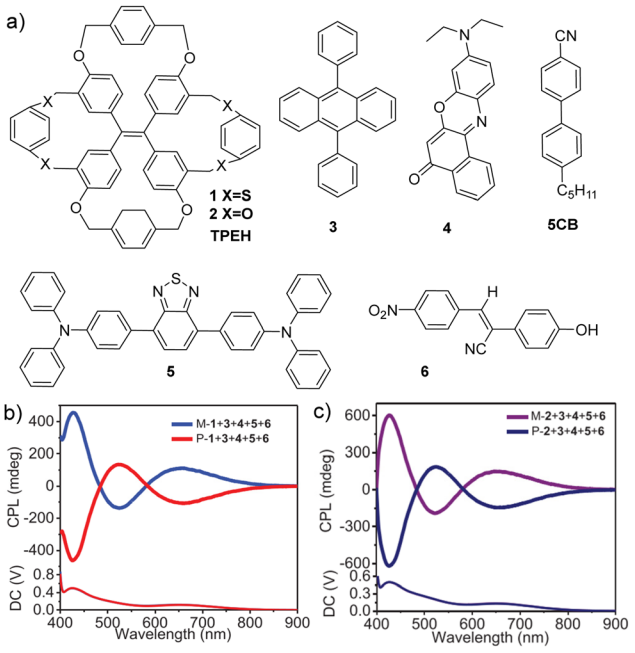

Fig. 23 (a) The structures of chiral inducers **TPEH 1** and **2**, achiral dyes **3**, **4**, **5** and **6,** and nematic liquid crystal 5CB. (b) The CPL spectra of ***M*/*P*-1-3-4-5-6-5CB**,and (c) ***P*/*M*-2-3-4-5-6-5CB**. Reproduced with permission from ref. 54. Copyright 2023, Wiley-VCH.

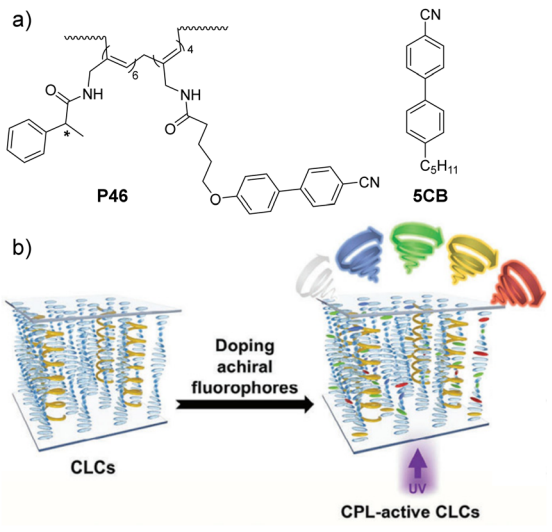

Fig. 24 (a) The molecular structures of chiral inducer **P46** and nematic liquid crystal **5CB**. (b) Schematic illustration of the preparation of full-color and white CPL-active CLCs. Reproduced with permission from ref. 55. Copyright 2025, Wiley-VCH.

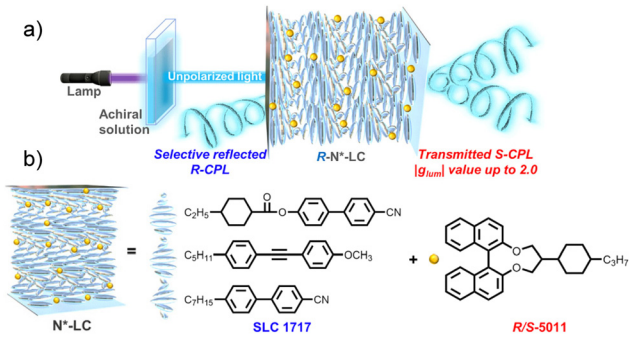

Fig. 25 (a) The selective reflection mechanism of N*-LCs. (b) The composition of the N*-LCs. Reproduced with permission from ref. 56. Copyright 2025, Springer Nature.

The N*-LCs were tailored to reflect different spectral regions by doping nematic liquid crystals with chiral inducers at optimized concentrations. Furthermore, full-color CPL emissions were realized by pairing these reflect bands with corresponding achiral luminophores, resulting in $|g_{PL}|$ values consistently exceeding 1.5 and approaching 2 in some instances. Besides, white-emission solution was constructed by doping complementary-color emitters in aqueous and toluene solution, yielding bright white emission with CIE coordinates of (0.31, 0.34) and (0.31, 0.35), respectively. White CPL emission was subsequently achieved by placing two N*-LC layers – selectively reflecting blue and yellow wavelengths – behind the white-light emitting solution. This multilayered configuration facilitated synergistic modulation of the emitted light's polarization state, leading to a significant amplification of the dissymmetry factor, with $|g_{PL}|$ values reaching up to 2.0. This study presented a general strategy for achieving both full-color and white CPL emissions with high dissymmetry factors, offering a promising platform for advanced applications in chiroptical displays.

In order to achieve high performance CPL simultaneously with high $|g_{lum}|$ values and high emission efficiency, our group recently proposed a strategy based on intrinsically luminescent N*-LC systems.[57] Full-color emissive films were fabricated by doping chiral inducers (***P*/*M*-THH**) into intrinsically luminescent liquid crystals (LLCs), including **2PFQ** (blue), **2PFBQ** (green), **2PFB** (yellow), **2PFSe** (orange), and **2PFS** (red) at optimized ratios (Fig. 26). The resulting chiral films exhibited nematic phases with high brightness (PLQYs, up to 99%) and outstanding CPL activity achieving $|g_{PL}|$ values of up to 0.75 following rapid thermal annealing. Furthermore, white-emission CPL films were constructed *via* co-doping mixtures of **2PFQ** and **2PFSe** (179 : 1) with chiral dopants, exhibiting bright white CPL signals with CIE coordinates of (0.33, 0.33) and $|g_{PL}|$ values also reaching 0.75. This study provided a new strategy for the construction of high-performance CPL-active materials based on N*-LC matrices, offering significant potential for application in next-generation chiroptical devices.

Through supramolecular self-assembly, host–guest systems, and chirality induction strategies, researchers have successfully achieved efficient and stable white circularly polarized light emission, providing a critical foundation for applications in 3D displays, optical data storage, and biosensing. Nevertheless, further improvement of $|g_{PL}|$ and enhancement of emission efficiency continue to be a crucial focus for future research endeavors.

4.2 WCPEL based on multi-component materials

In the field of chiral metal complexes, lanthanide-based complexes have attracted significant attention due to their characteristic f–f transitions. Since magnetic dipole transitions are allowed while electric dipole transitions are forbidden in lanthanides, these complexes typically exhibit large luminescence dissymmetry. In 2023, Wong *et al.* reported the first CP-WOLED device employing chiral organolanthanide complex **[Sm(tta)$_3$(D-phen)]** as an emitter, achieving an EQE_{max} of 1.55% and a $|g_{EL}|$ of 0.011 (Fig. 27).[58] Under photoexcitation, **Sm(tta)$_3$(D-phen)** demonstrated efficient orange emission with remarkable CPL activity. Furthermore, CP-WOLEDs based on **Sm(tta)$_3$(D-phen)** were fabricated, whose emissive layer was formed by doping **Sm(tta)$_3$(D-phen)** into a PVK-PBD polymer host matrix (Fig. 27b). The devices achieved white-light emission at a turn-on voltage of 7.0 V, with CIE coordinates of (x = 0.268–0.297, y = 0.203–0.224), a CCT of 2625–2631 K, and a CRI of 96–97. This work represented the first demonstration of CP-WOLEDs based on the chiral lanthanide complexes, presenting relatively large $|g_{lum}|$ values. However, the overall device efficiency remained relatively low, likely attributable to the relatively low PLQY.

On the other hand, due to the diversity and environmental friendliness of purely organic chiral luminescent materials, CP-WOLEDs based on such materials have also been extensively studied. In 2021, Cheng *et al.* successfully fabricated

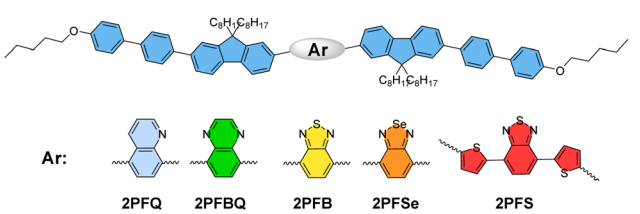

Fig. 26 The structures of achiral nematic liquid crystals **2PFQ**, **2PFBQ**, **2PFB**, **2PFSe** and **2PFS**.

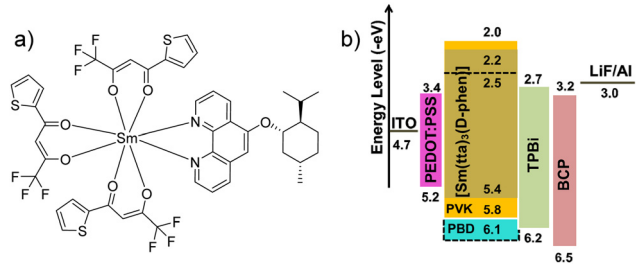

Fig. 27 (a) The structure of chiral organo-Sm^{3+} complex **[Sm(tta)$_3$(D-phen)]**. (b) The device structure of CP-WOLEDs.

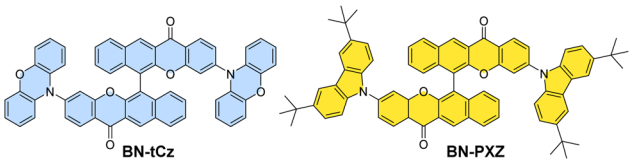

Fig. 28 The molecular structures of **BN-tCz** and **BN-PXZ**.

complementary multi-component CP-WOLEDs for the first time (Fig. 28).[11] By co-doping blue-emitting axially chiral organic emitters (***S***-/***R***-**BN-*t*CZ**) with orange-emitting axially chiral organic emitters (***S***-/***R***-**BN-PXZ**) in a single emission layer, solution-processed CP-WOLED devices were fabricated, which exhibited warm-white electroluminescence with CIE coordinates of (0.32, 0.45), an EQE_{max} of 0.8%, and an L_{max} of 10 200 cd m^{-2}. Furthermore, the electroluminescence spectra of CP-WOLEDs exhibited little change with varying voltages. Additionally, CP-WOLED devices exhibited mirror-image CPEL signals with a $|g_{EL}|$ value of 2.14×10^{-3}. Although the overall performance parameters of this device still require further improvement, this study provided significant theoretical insights into the development of CP-WOLED devices (Table 2).

In 2024, this group also developed a chiral co-assembly-sensitized circularly polarized luminescence (CCS-CPL) strategy to enhance the comprehensive performance of CP-WOLEDs (Fig. 29).[59] The chiral co-assembly sensitizer $(S\text{-}/R\text{-Cz})_{0.2}$-$(I\text{-P})_{0.8}$ was developed by leveraging the π···π stacking interactions between chiral binaphthyl derivatives ***S***-/***R***-**Cz** and achiral conjugated pyrene-based polymer ***I***-**P**. Furthermore, by incorporating chiral co-assembly sensitizer $(S\text{-}/R\text{-Cz})_{0.2}$-$(I\text{-P})_{0.8}$ along with full-color achiral aggregation-induced emission (AIE) dyes into the single-emission layer, solution-processed CP-WOLED devices were prepared, which exhibited color-tunable WCPEL with CIE coordinates of (0.33, 0.33), a CRI of 93, a $|g_{EL}|$ value of 0.071, an EQE_{max} of 0.66%, and an L_{max} of 4588 cd m^{-2}. Meanwhile, the solution-processed CP-WOLEDs exhibited excellent spectra stability with different voltages. This is the first report of CP-WOLEDs using the CCS-CPL strategy, providing a new strategy for the fabrication of high-performance white CP-EL devices. However, the EQE_{max} was still limited to 0.66%, which could be ascribed to the use of fluorescence materials.

To furthermore improve the efficiency of CP-WOLEDs, Zheng *et al.* fabricated dual-emission-layer CP-WOLEDs by employing chiral TADF materials as complementary emitters.[13] Spirofluorene-based chiral blue TADF material ***S***-/***R***-**OSFSO** and spirofluorene-based chiral orange TADF material

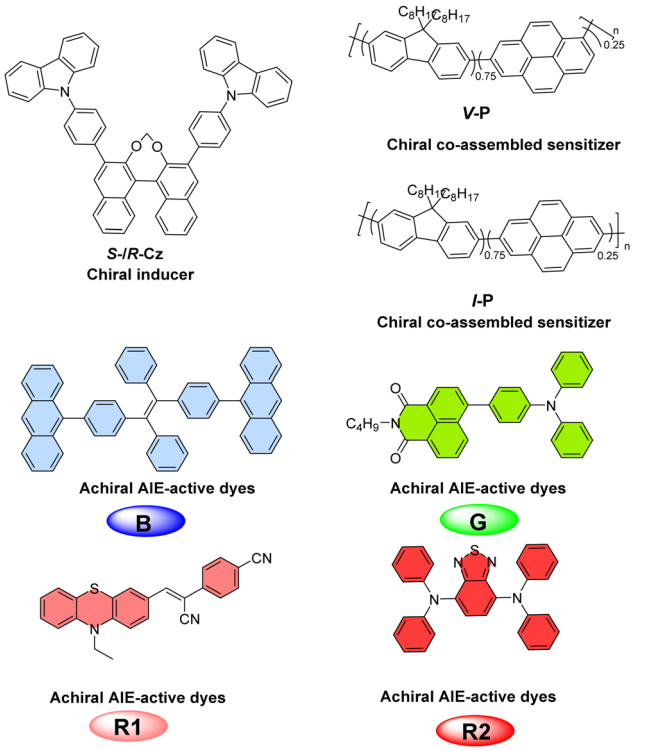

Fig. 29 The molecular structures of chiral inducer ***S*/*R*-Cz**, chiral co-assembled sensitizers ***I*-P** and ***V*-P**, and achiral dyes **B**, **G**, **R1** and **R2**.

S-/***R***-**SPOCN** were selected as complementary emitters for the fabrication of dual-emission-layer CP-WOLED devices (Fig. 30). The resulting device exhibited warm-white electroluminescence with CIE coordinates of (0.35, 0.46), achieving an EQE_{max} of 21.6%, a $|g_{EL}|$ value of 3.0×10^{-3}, a CRI of 69, and an L_{max} of 15 700 cd m^{-2} (Fig. 30(b)). In this study, a dual-TADF dopant strategy was adopted to simultaneously harvest singlet (S_1) and triplet (T_1) excitons, thereby markedly enhancing exciton utilization and enabling efficient CPEL. Despite these advances, the device exhibited a relatively low CRI and a modest $|g_{EL}|$ value, which collectively constrain its applicability in high-performance display and lighting technologies.

In 2025, this group further advanced the development of CP-WOLEDs by designing intrinsically chiral TADF materials to improve $|g_{lum}|$ values.[60] The intrinsically chiral orange-emitting TADF materials, **D8TPN**, were synthesized *via* the Heck coupling reaction, which exhibited a $|g_{PL}|$ value of 7×10^{-3} (Fig. 30). Subsequently, the CP-WOLED device using single-emission layer was constructed by co-doping achiral blue-emitting host material **DMIC-TRZ** with the chiral orange-

Table 2 WCPEL performance based on multi-component materials

Entry	Emitters	CIE coordinates	CRI	$\|g_{EL}\|$	L_{max} (cd m^{-2})	EQE_{max} (%)	Ref.
1	**$Sm(tta)_3$(D-phen)**	(0.30, 0.22)	96	0.011	—	1.55	58
2	**(*S*-/*R*-BN-*t*CZ)-(*S*-/*R*-BN-PXZ)**	(0.32, 0.45)	—	2.14×10^{-3}	10 200	0.8	11
3	**B-G-R1-R2**	(0.33, 0.33)	93	0.071	4588	0.66	59
4	**(*S*-/*R*-OSFSO)-(*S*-/*R*-SPOCN)**	(0.35, 0.46)	69	3.0×10^{-3}	15 700	21.6	13
5	**(D8TPN)-(DMIC-TRZ)**	(0.29, 0.28)	—	1.5×10^{-3}	12 103	12.8	60

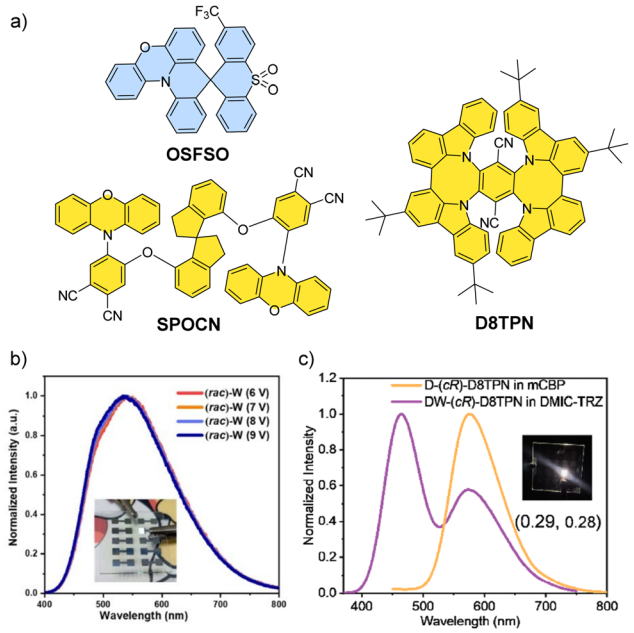

Fig. 30 (a) The molecular structures of chiral TADF materials **OSFSO**, **SPOCN** and **D8TPN**. (b) Voltage-dependent EL spectra of CP-WOLED devices. (c) EL spectra of CP-WOLED devices and OLED devices employing **D8TPN** as an emitter. Reproduced with permission from ref. 13. Copyright 2022, Wiley-VCH. Reproduced with permission from ref. 60. Copyright 2025, Wiley-VCH.

emitting emitters **D8TPN**. The resulting device exhibited cold-white WCPEL with CIE coordinates of (0.29, 0.28), achieving an EQE_{max} of 12.8%, a $|g_{EL}|$ value of 1.5×10^{-3}, and an L_{max} of 12,103 cd m^{-2} (Fig. 30(c)). This study provided a molecular-level approach to enhance the $|g_{lum}|$ value of WCPL. However, the use of achiral blue emitters, while necessary for color balancing, may compromise the overall $|g_{EL}|$ value due to the absence of intrinsic chirality.

Although the design strategy of incorporating dual TADF emitters and the dual-emission-layer structure effectively enhances the EQE_{max} of CP-WOLED devices, the fabrication of CP-WOLEDs through the complementary emission of multiple emissive dopants inherently faces several limitations including self-absorption, high production costs, and emission instability.[61] Therefore, the development of novel material systems and device architectures to overcome these existing limitations has become a crucial research direction in this field.

5. WCPL based on single-component materials

Compared to multi-component WCPL systems, single-component WCPL systems offer significant advantages, including simplified molecular design, reduced risk of phase separation, and improved device stability. As a result, single-component WCPL has attracted widespread attention in recent years. To achieve efficient single-component WCPL, current design strategies primarily focus on (i) constructing chiral complexes incorporating multiple emissive centers, (ii) designing chiral molecules capable of excimer formation, and (iii) developing chiral frameworks with multiple conformations. The following sections will systematically elaborate on single-component WCPL from the perspectives of material design strategies, luminescence mechanisms, research progress, and existing challenges.

5.1 WCPPL based on single-component materials

5.1.1 WCPPL based on single-component organic–inorganic hybrid materials. The unique combination of inorganic frameworks and chiral organic cations endows hybrid perovskites with broad emission capability and chiroptical functionality, offering a versatile molecular design strategy for CPL-active white-light systems. In 2018, Luo *et al.* reported a single-component white-emission chiral one-dimensional organic–inorganic hybrid perovskite material $C_5H_{14}N_2PbCl_4 \cdot H_2O$ (**1**), featuring a quantum-wire structure composed of edge-shared highly distorted lead chloride octahedra (Fig. 31(a)).[23] The material exhibited complementary dual-emission characteristics, featuring a high-energy emission band at 412 nm upon excitation at 360 nm and a distinct low-energy emission band at 617 nm under 330 nm excitation. As the excitation wavelength decreased from 360 nm to 330 nm, the intensity of 412 nm emission decreased, while that of 617 nm emission increased (Fig. 31(b)). Under 344 nm excitation, **1** exhibited warm-white emission with CIE coordinates of (0.39, 0.37), a CCT of 3445 K, a CRI of 93.9, and a PLQY of 1%. Subsequent experimental studies demonstrated that **1** exhibited red emission at 617 nm *via* self-trapped excitons (STEs) in a distorted lattice, while the organic component contributed to the blue emission at 412 nm. Moreover, owing to the incorporation of

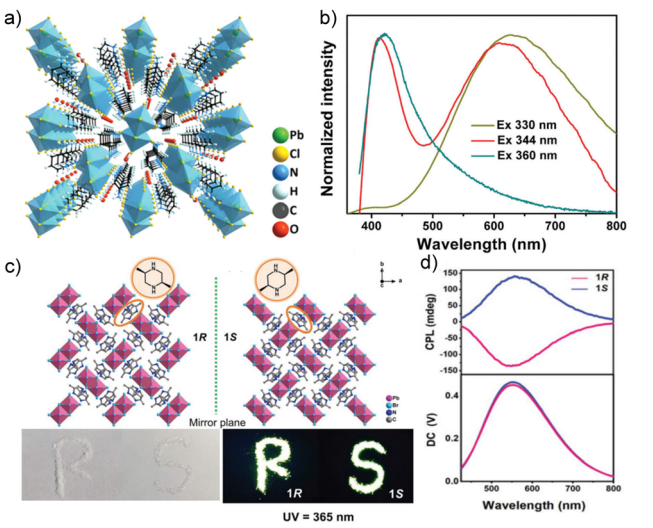

Fig. 31 (a) Packing framework of **1**. (b) Emission spectra of the microscale perovskite crystals at different excitation wavelengths. (c) Crystal structures of **1*R*** and **1*S***. (d) WCPPL and DC curves of **1*R*** and **1*S***. Reproduced with permission from ref. 23. Copyright 2018, Royal Society of Chemistry. Reproduced with permission from ref. 24. Copyright 2023, Wiley-VCH.

chiral pure organic cations, this material exhibited circularly polarized optical activity. Although the PLQY remains relatively low, this study provided a novel strategy for the design of chiral white-emission hybrid perovskites.

The $|g_{lum}|$ values of chiral perovskites induced by the chiral organic molecular cations were usually only on the order of 10^{-4}–10^{-3}. To address this limitation and enhance the performance of WCPL, Zhang *et al.* developed a synergistic strategy that integrates STE emission with the host–guest type chiral induction interaction strategy (Fig. 31(c)).[24] This approach enabled the construction of chiral one-dimensional double-chain perovskites, **(*RR*/*SS*-DMPZ)PbBr$_4$**, formed by distorted octahedral units. These perovskites exhibited single-component WCPL emission with CIE coordinates of (0.36, 0.41), a CCT of 4759 K, and a CRI of 77. In addition, the PLQY of **(*RR*/*SS*-DMPZ)PbBr$_4$** was improved to 28.4%, which is attributed to the short Pb–Pb structural distances. Meanwhile, mirror-image WCPPL spectra were observed with a $|g_{lum}|$ of 2.32×10^{-2} (Fig. 31(d)). Furthermore, WLED devices were fabricated by coating **(*RR*/*SS*-DMPZ)PbBr$_4$** powder onto commercial 365 nm LED chips. The WLED devices showed bright white light with CIE coordinates of (0.36, 0.41), a CRI of 78, and a color temperature of 4708 K.

Additionally, without the need for any external chiral inducers or applied physical fields, spontaneous chiral induction can be achieved solely through the self-assembly of achiral components. In 2022, Hong *et al.* prepared asymmetric assembly of **1-M** and **1-P** through the coordination between achiral Hptdp ligands and Cu_2I_2 clusters.[10] **1-M** and **1-P** exhibited the intrinsic integration of white-light emission and CPL properties. Notably, the chirality does not originate from any inherent asymmetry in the molecular skeleton, but rather arises from conformational locking of the ligand during coordination and the cooperative effect of spatial packing (Fig. 32(a)). Moreover, under 350 nm excitation, mirror-image CPL signals of **1-M** and **1-P** in the single-crystal state were detected with a $|g_{PL}|$ value of 8×10^{-3} (Fig. 32(c)). Besides, **1** exhibited tunable dual emission bands, the intensities of which varied with the excitation wavelength (Fig. 32(b)). Under 400 nm excitation, **1** displayed warm white-light emission with CIE coordinates of (0.42, 0.42), a PLQY of 2.4%, a CCT of 3492 K, and a CRI of 90.8. Furthermore, **1** was coated onto a 380 nm LED chip, successfully fabricating a warm white-light LED device with CIE coordinates of (0.41, 0.41) and a CRI of 93.4. This marked the first instance of simultaneously achieving single-component white-light emission and CPL in a coordination polymer.

5.1.2 WCPPL based on single-component purely organic materials. In 2017, Bari *et al.* constructed chiral naphthalene diimide **NDI 3** by introducing chiral groups onto the carboxylated naphthalene diimide framework, which exhibited WCPPL in both solution and thin-film states[62] (Fig. 33(a)). In the supramolecular aggregate state, **NDI 3** exhibited white emission with CIE coordinates of (0.26, 0.34), and its $|g_{PL}|$ values reached 2×10^{-2} at 470 nm and 1×10^{-2} at 555 nm, significantly surpassing most reported $|g_{PL}|$ values for organic small molecules. Furthermore, **NDI 3** dissolved as single molecules in dipolar solvents such as chloroform, whereas in nonpolar solvents such as cyclohexane, it self-assembled into supramolecular aggregates through π···π stacking and hydrogen bonding interactions. In this aggregated state, an unstructured emission band was observed, indicating the formation of excimers. Additionally, when the proportion of nonpolar solvent reached 80%, the formation of J-type π-stacking was observed, as evidenced by the redshift and hypochromic effect in the UV-Vis absorption spectrum. This study represented the first report of a single-component WCPPL system based on small molecules, holding significant scientific importance. However, it was regrettable that the authors did not attempt to fabricate CP-WOLED devices based on this system.

In 2022, Duan *et al.* synthesized a pair of white-emission CPL-active enantiomers, ***R*-/*S*-1**, incorporating chiral 2-aminocyclohexanol into a guanidine-substituted 1,8-naphthalimide fluorophore.[63] These enantiomers exhibited solvent-dependent luminescence behaviors.

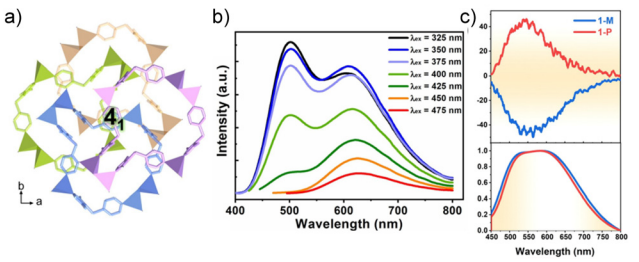

Fig. 32 (a) The helical packing mode of **1-M** along the *b* axis. (b) Excitation-dependent photoluminescence spectra of **1**. (c) CPL spectra and DC curves of **1-M** and **1-P** in the single-crystal state. Reproduced with permission from ref. 10. Copyright 2022, Wiley-VCH.

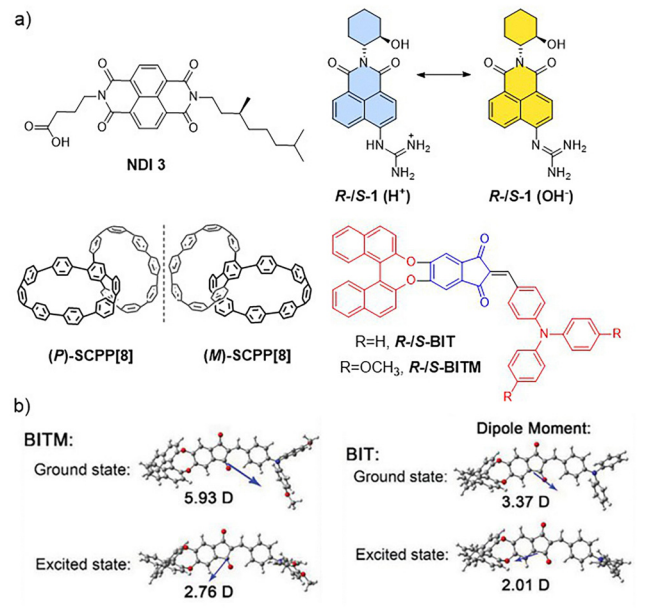

Fig. 33 (a) The molecular structures of **NDI3**, ***R*-/*S*-1**, **(*M*/*P*)-SCPP[8]**, ***R*-/*S*-BIT** and ***R*-/*S*-BITM**. (b) The dipole moments of **BIT** and **BITM** in various electronic states. Reproduced with permission from ref. 61. Copyright 2024, Wiley-VCH.

The emission color of ***R*-/*S*-1** could be tuned by adjusting the pH, shifting from blue in an acidic aqueous solution to yellow under alkaline conditions (Fig. 33(a)). At neutral polarity, the enantiomers displayed white circularly polarized luminescence. These phenomena were attributed to the synergistic effect of excited-state proton transfer in the guanidine moiety and intramolecular charge transfer within the naphthalimide group. Furthermore, ***R*-/*S*-1** exhibited mirror-image WCPL signals in a neutral aqueous solution with $|g_{PL}|$ on the order of 10^{-4}. This study represented the first report of single-molecule WCPL achieved by regulating the ESPT behavior.

In 2022, Du *et al.* reported chiral dual-emission macrocycles **(*M*/*P*)-SCPP[8]**, which integrate the 1,2,4,5-tetraphenylbenzene core with a rigid macrocycle to form a rigid bismacrocycle structure (Fig. 33).[16] This structurally constrained system demonstrated remarkable AIE characteristics with tunable dual emission, exhibiting a PLQY of 3% with anthracene as a reference in ethanol. In tetrahydrofuran (THF) solution, **SCPP[8]** exhibited cyan fluorescence at 475 nm, while aggregation induced a bathochromic shift to orange emission at 577 nm. Notably, in the THF/H_2O mixture with a 60% water content, **SCPP[8]** exhibited near-white light emission with CIE coordinates of (0.33, 0.37). The observed emission modulation arises from a delicate balance between competing aggregation-caused quenching and AIE phenomena. Additionally, **(*M*/*P*)-SCPP[8]** exhibited enhanced chiroptical performance in the aggregated state, with the $|g_{PL}|$ increasing from 6.9×10^{-3} (solution) to 1.9×10^{-2} (aggregated state), outperforming most reported organic small molecules.

In 2023, Yao *et al.* reported two axially chiral binaphthol-based derivatives, ***R*-/*S*-BIT** and ***R*-/*S*-BITM**, by integrating axially chiral binaphthol (BINOL) with a deep-red-emitting chromophore (Fig. 33(a) and (b)).[64] Remarkably, ***R*-/*S*-BIT** demonstrated single-molecule white emission with CIE coordinates of (0.33, 0.34) in toluene solution, whereas ***R*-/*S*-BITM** shows near-infrared (NIR) emission in the powder state. This pronounced photophysical divergence arises from donor-modulated dipole moments, which govern the intramolecular charge transfer efficiency (Fig. 33(b)). Furthermore, comprehensive density functional theory (DFT) calculations coupled with photophysical analyses revealed that ***R*-/*S*-BIT**'s dual emission stems from (i) higher-energy bands arising from localized excited (LE) states and (ii) lower-energy emission originating from the twisted intramolecular charge transfer process with substantial structural reorganization.

An alternative strategy for constructing single-molecule WCPL materials involves the design of chiral luminophores with multiple thermodynamically stable conformations. By precisely modulating the conformer population, white emission can be achieved *via* an intramolecular "self-doping" mechanism. Based on this strategy, in 2024, Ma *et al.* successfully synthesized a multi-conformation molecule, **DG/LG-DPAC**, by integrating *N*,*N*′-disubstituted dihydrophenazine units (**DPAC**) with vibration-induced emission (VIE) characteristics and chiral dialkyl glutamylamide moieties within a single molecular framework (Fig. 34(a)).[9] Furthermore, supramolecular gels based on **DG/LG-DPAC** were subsequently fabricated,

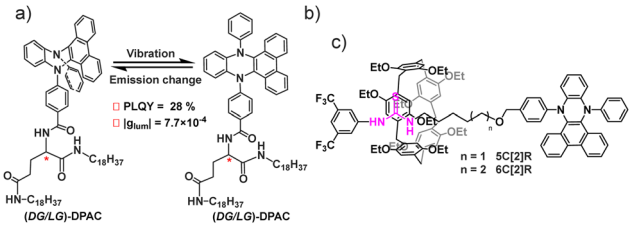

Fig. 34 (a) The molecular structures of **DG/LG-DPAC** in different conformers. (b) The molecular structures of **5C[2]R** and **6C[2]R**.

exhibiting solvent-dependent CPL: orange-red emission ($|g_{PL}| = 7.3 \times 10^{-4}$) in toluene, near-white emission ($|g_{PL}| = 6.7 \times 10^{-4}$) in ethyl acetate, and blue emission ($|g_{PL}| = 7.7 \times 10^{-4}$) in methanol. Comprehensive studies revealed that the fluorescence color variation originated from self-assembly-induced microstructural changes. Specifically, through intramolecular vibrations, the molecular configuration of **DG/LG-DPAC** tended to transform from a bent shape to a planar shape, resulting in orange-red fluorescence upon excitation. Besides, based on its multi-color CPL properties, a multi-dimensional encoding system was constructed, achieving multi-level information storage and encryption functionalities. This study provided new insights into the design of single-molecule WCPL materials and their potential applications in information security and anti-counterfeiting technologies.

In the same year, Yang *et al.* reported a dual-stimuli-responsive [2]rotaxane system (**5C[2]R** and **6C[2]R**), featuring **DPAC** as a terminal luminogen, which exhibited tunable emission and switchable CPL (Fig. 34(b)).[65] Anion-driven ring shuttling modulated the CPL intensity with excellent reversibility, while solvent viscosity controlled the VIE behavior, enabling a transition from orange-red to white and eventually blue emission. Furthermore, embedding the chiral rotaxane into a stretchable polymer matrix yielded flexible thin films with white-light emission. Upon mechanical stretching, the emission color shifted from white to blue, accompanied by a 6.5-fold increase in the $|g_{PL}|$ value. This study presented a robust design strategy for constructing stimuli-responsive chiral luminophores and offered a promising platform for advanced smart photonic materials.

5.2 WCPEL based on single-component materials

Although previous reports have achieved single-molecule WCPPL through some strategies, none of them have been able to achieve WCPL at the device level. In 2024, our group reported the design and synthesis of single-molecule WCPL materials, ***R*-/*S*-DO-PTZ**, by integrating conformationally switchable phenothiazine-based donors with chiral acceptor units (Fig. 35(a)).[66] The resulting ***R*-/*S*-DO-PTZ** exhibited complementary dual-emission behavior with CIE coordinates of (0.30, 0.33), comprising a blue fluorescence band originating from the ax–ax conformer and a yellow TADF band from the ax–eq conformer. Notably, mirror-image CPL signals were observed, with $|g_{PL}|$ values reaching 3.0×10^{-3}. Furthermore, CP-WOLEDs were fabricated using ***R*-/*S*-DO-PTZ** as an emitter.

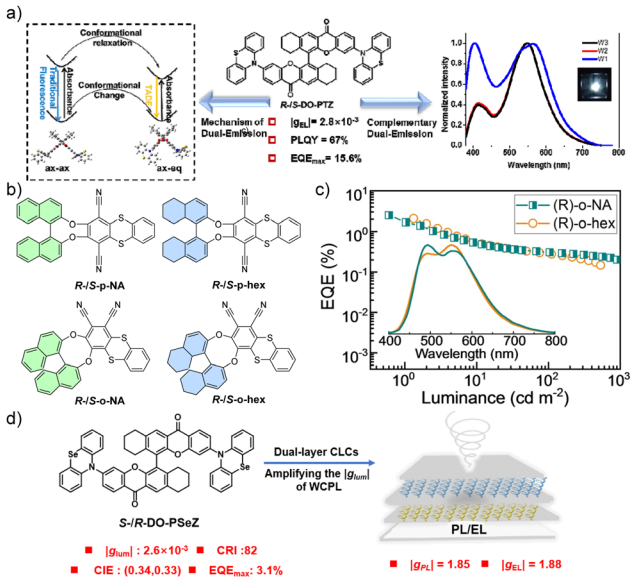

Fig. 35 (a) The scheme of single-molecule WCPL and WCPEL from the dual-emission mechanism. (b) The molecular structure of ***R*-/*S*-p-NA**, ***R*-/*S*-p-hex**, ***R*-/*S*-o-NA** and ***R*-/*S*-o-hex**. (c) The EQE–luminance curves of the WCPEL device with ***R*-/*S*-o-NA** and ***R*-/*S*-o-hex** as emitters, respectively. (d) Conceptual representation of a universal strategy for amplifying the g_{lum} values in both WCPPL and WCPEL *via* Bragg reflection from dual-layer CLCs. Reproduced with permission from ref. 67. Copyright 2025, Wiley-VCH.

These devices delivered bright white CPEL with CIE coordinates of (0.32, 0.37), a CRI of 73, and an EQE_{max} of 4.7%. To enhance device performance, dual-host architectures were developed, yielding warm-white CPEL with a $|g_{EL}|$ value of 2.8×10^{-3}, CIE coordinates of (0.37, 0.48), and an EQE_{max} of up to 15.6%. Meanwhile, all the CP-WOLEDs exhibited stable electroluminescence spectra. This work represented the first demonstration of CP-WOLEDs based on single-molecule purely organic emitters, providing a promising strategy for the development of high-performance single-molecule CP-WOLEDs (Table 3).

In 2024, Su *et al.* synthesized chiral molecules ***R*-/*S*-p-NA**, ***R*-/*S*-p-hex**, ***R*-/*S*-o-NA** and ***R*-/*S*-o-hex** *via* chalcogen-bridged (S/Se) isomer engineering (Fig. 35(b)).[67] Among them, ***R*-/*S*-o-NA** and ***R*-/*S*-o-hex** exhibited synergistic TADF/room-temperature phosphorescence (RTP) dual emission, attributed to enhanced spin–orbit coupling and vibronic spin–orbit coupling effects. Furthermore, CP-WOLED devices employing these dual-emission molecules as emitters were fabricated, achieving single-molecule warm white electroluminescence. Specifically, the device utilizing ***R*-/*S*-o-NA** as an emitter exhibited an EQE_{max} of 2.1% with CIE coordinates of (0.34, 0.43), while the device based on ***R*-/*S*-o-hex** showed an EQE_{max} of 2.5% and CIE coordinates of (0.33, 0.43) (Fig. 35(c)). This represented the first example of single-molecule WOLEDs based on the dual-emission mechanism of TADF and phosphorescence. However, the relatively low efficiency of these devices was presumably attributed to the long lifetime of the phosphorescent component, which leads to triplet exciton annihilation.

To further improve the CRI value of CP-WOLEDs, in 2025, our group further designed single-molecule multi-emission materials, ***R*-/*S*-DO-PSeZ**, by integrating conformationally switchable phenoselenazine-based donors with chiral carbonyl-containing acceptor units (Fig. 35(d)).[68] This pair of enantiomers exhibited white phosphorescence emission with CIE coordinates of (0.33, 0.34) and a PLQY of 42%. Detailed conformational analysis revealed that the multi-emissive characteristics originated from three conformers: the quasi-axial/quasi-axial/*cis* (ax–ax–*cis*) conformer contributed to blue phosphorescence, the quasi-axial/quasi-axial/*trans* (ax–ax–*trans*) conformer emitted yellow phosphorescence, and the quasi-axial/quasi-equatorial (ax–eq) conformer was responsible for red phosphorescence. Furthermore, CP-WOLEDs employing ***R*-/*S*-DO-PSeZ** as an emitter were fabricated, demonstrating triple-emission WCPEL with the CIE coordinates of (0.29, 0.33), a CRI of 82, an EQE_{max} of 3.1% and a $|g_{EL}|$ value of 2.8×10^{-3}. Furthermore, a universal chiroptical enhancement strategy was established based on the Bragg reflection effect of dual-layer CLCs, which was applied to both photoluminescent and electroluminescent systems (Fig. 35(d)). As a result, the $|g_{PL}|$ and $|g_{EL}|$ reached 1.85 and 1.88, respectively, representing the highest reported values for WCPEL to date. This work not only provided an effective molecular design strategy for constructing high-performance single-molecule multi-emission materials but also offered a novel perspective for the advancement of next-generation WCPPL and WCPEL devices with superior chiroptical and color-rendering properties.

Despite advantages such as simple preparation and stable emission colors, the development of single-component WCPL materials remains in its infancy due to intrinsic challenges in molecular design. Currently reported systems are still limited in number and exhibit several limitations, particularly their generally low $|g_{lum}|$ values, which require further enhancement through molecular engineering or supramolecular assembly strategies.

4. Conclusions and perspectives

In summary, significant progress has been made in the development of WCPL systems, encompassing a wide variety of

Table 3 WCPEL performance based on single-component materials

Entry	Emitters	CIE coordinates	CRI	$\|g_{EL}\|$	L_{max} (cd m^{-2})	EQE_{max} (%)	Ref.
1	***R*-/*S*-DO-PTZ**	(0.32, 0.37)	73	2.8×10^{-3}	803	4.7	66
2	***R*-/*S*-o-NA**	(0.34, 0.43)	—	—	—	2.1	67
3	***R*-/*S*-o-hex**	(0.33, 0.43)	—	—	—	2.5	67
4	***R*-/*S*-DO-PSeZ**	(0.29, 0.33)	82	2.8×10^{-3} [a]/1.88[b]	2066	3.1	68

[a] The $|g_{EL}|$ value measured on intrinsically chiral devices. [b] The $|g_{EL}|$ value measured on multi-layer devices equipped with CLCs.

material platforms such as macrocyclic compounds, liquid crystal composites, quantum dots, nanoparticles, polymers, metal complexes, and microcrystals. Meanwhile, the applications of WCPL materials have been widely explored in various fields. In this review, we have systematically elaborated the design strategies of WCPL materials, including polymer-based systems for white-light generation, multicomponent doping approaches to construct broadband emissive systems, and single-component emitters that exhibited complementary multi-emission at the molecular level. These methodologies have dual significance: (i) fundamentally expanding the theoretical paradigm for functional material design and (ii) establishing a library of tunable protocols that enable precision engineering of luminescence characteristics for targeted application scenarios. Besides, from the perspective of luminescence mechanisms, WCPL materials span phosphorescence, traditional fluorescence, and TADF mechanisms, where phosphorescence and TADF mechanisms can achieve a theoretical IQE of 100% by fully harvesting both singlet and triplet excitons. Among the three representative strategies for constructing WCPL materials, polymer-based systems can achieve a high CRI exceeding 90; however, their maximum $|g_{lum}|$ values remain at the 10^{-2} level. In multicomponent-doped systems, liquid crystal-based assemblies can effectively amplify $|g_{lum}|$ values close to the ideal value of 2 through Bragg reflection from CLCs. Nevertheless, this approach involves complex fabrication processes and is susceptible to phase separation. In contrast, single-component WCPL systems offer simplified preparation and inherently avoid phase separation issues, yet the intrinsic $|g_{lum}|$ values are generally low and rely heavily on sophisticated molecular design to simultaneously achieve white-light emission and chiroptical activity.

Despite substantial advances in WCPL materials, the field remains in a nascent developmental stage, harboring significant untapped potential for both fundamental breakthroughs and technological innovation. High-performance WCPL materials should simultaneously fulfill several key criteria: facile processability, a high $|g_{lum}|$ value, high PLQY, and superior white-light characteristics, including broad spectral coverage and a high CRI value. The future development of WCPL materials should mainly focus on three aspects: the development of high-performance WCPL materials; exploration of their applications in a wider range of fields, particularly in electroluminescent devices; and promotion of the industrial applications of WCPL materials. First, developing innovative material design methodologies constitutes a critical pathway to high-performance WCPL materials. Promising approaches include the construction of WCPL polymers incorporating both TADF properties and self-assembly capabilities, the integration of multiple designing strategies to achieve concurrently high $|g_{lum}|$ values and strong emission efficiency in WCPL materials, the development of WCPL polymers or small molecules exhibiting intrinsic luminescence liquid crystalline properties and the exploration of persistent luminescent (long-afterglow) WCPL systems. These approaches offer opportunities to expand the structural diversity and optimize the photophysical properties of WCPL materials. Beyond fundamental material development, broadening the functional applications of WCPL systems, especially in electroluminescent devices, is equally crucial. Incorporating cholesteric liquid crystals with Bragg reflection ability into high-efficiency white-emission devices presents an attractive approach to enhance the performance of WCPEL. Moreover, controlling the molecular orientation and hierarchical assembly of liquid crystalline polymers or small molecules within device architectures is anticipated to facilitate the construction of multifunctional and structurally adaptable optoelectronic devices. Critically, transitioning high-performance WCPL materials to industrial production is vital for next-generation displays. Integrating these materials into micro/nano photonic devices could unlock numerous technological opportunities across various fields, including 3D displays, biomedical diagnostics, asymmetric catalysis, and information storage. With continuous innovation in the design of chiral luminescent materials and rapid advancements in relevant fabrication technologies, we believe that WCPL materials will soon become a focus of cutting-edge research and practical applications.

Conflicts of interest

There are no conflicts to declare.

Data availability

No supporting data are included in this article.

Acknowledgements

We thank the National Natural Science Foundation of China (92256304 and 22371277) and the Ministry of Science and Technology of China (2022YFA1204401) for financial support.

Notes and references

1 A. M. T. Muthig, O. Mrózek, T. Ferschke, M. Rödel, B. Ewald, J. Kuhnt, C. Lenczyk, J. Pflaum and A. Steffen, *J. Am. Chem. Soc.*, 2023, **145**, 4438–4449.
2 Z. A. VanOrman, W. R. Kitzmann, A.-P. M. Reponen, T. Deshpande, H. J. Jöbsis and S. Feldmann, *Nat. Rev. Chem.*, 2025, **9**, 208–223.
3 F. Furlan, J. M. Moreno-Naranjo, N. Gasparini, S. Feldmann, J. Wade and M. J. Fuchter, *Nat. Photonics*, 2024, **18**, 658–668.
4 J. M. Moreno-Naranjo, F. Furlan, J. Wang, S. T. J. Ryan, T. Matulaitis, Z. Xu, Q. Zhang, L. Minion, M. Di Girolamo, T. Jávorfi, G. Siligardi, J. Wade, N. Gasparini, E. Zysman-Colman and M. J. Fuchter, *Adv. Mater.*, 2024, **36**, 2402194.
5 D.-W. Zhang, M. Li and C.-F. Chen, *Chem. Soc. Rev.*, 2020, **49**, 1331–1343.
6 L. Wan, Y. Liu, M. J. Fuchter and B. Yan, *Nat. Photonics*, 2023, **17**, 193–199.

7 Y. Liu, M. Nishiura, Y. Wang and Z. Hou, *J. Am. Chem. Soc.*, 2006, **128**, 5592–5593.
8 V. Anand, R. Mishra and Y. Barot, *Dyes Pigm.*, 2021, **191**, 109390.
9 Y. Hu, Z. Huang, I. Willner and X. Ma, *CCS Chem.*, 2024, **6**, 518–527.
10 M.-X. Yu, C.-P. Liu, Y.-F. Zhao, S.-C. Li, Y.-L. Yu, J.-Q. Lv, L. Chen, F.-L. Jiang and M.-C. Hong, *Angew. Chem., Int. Ed.*, 2022, **61**, e202201590.
11 Y. Zhang, J. Li, Y. Quan, S. Ye and Y. Cheng, *Chem. – Eur. J.*, 2021, **27**, 589–593.
12 Y. Zhang, Y. Li, Y. Quan, S. Ye and Y. Cheng, *Angew. Chem., Int. Ed.*, 2023, **62**, e202214424.
13 Y.-P. Zhang, M.-X. Mao, S.-Q. Song, Y. Wang, Y.-X. Zheng, J.-L. Zuo and Y. Pan, *Angew. Chem., Int. Ed.*, 2022, **61**, e202200290.
14 H.-R. Fu, N. Wang, X.-X. Wu, F.-F. Li, Y. Zhao, L.-F. Ma and M. Du, *Adv. Opt. Mater.*, 2020, **8**, 2000330.
15 Y. Cheng, S. Liu, F. Song, M. Khorloo, H. Zhang, R. T. K. Kwok, J. W. Y. Lam, Z. He and B. Z. Tang, *Mater. Horiz.*, 2019, **6**, 405–411.
16 X. Zhang, H. Liu, G. Zhuang, S. Yang and P. Du, *Nat. Commun.*, 2022, **13**, 3543.
17 K. Watanabe, I. Osaka, S. Yorozuya and K. Akagi, *Chem. Mater.*, 2012, **24**, 1011–1024.
18 Y. Li, K. Yao, Y. Chen, Y. Quan and Y. Cheng, *Adv. Opt. Mater.*, 2021, **9**, 2100961.
19 S. Huo, P. Duan, T. Jiao, Q. Peng and M. Liu, *Angew. Chem., Int. Ed.*, 2017, **56**, 12174–12178.
20 M. Li, C. Zhang, L. Fang, L. Shi, Z. Tang, H.-Y. Lu and C.-F. Chen, *ACS Appl. Mater.*, 2018, **10**, 8225–8230.
21 K. Watanabe, T. Sakamoto, M. Taguchi, M. Fujiki and T. Nakano, *Chem. Commun.*, 2011, **47**, 10996–10998.
22 L. Xu, C. Wang, Y.-X. Li, X.-H. Xu, L. Zhou, N. Liu and Z.-Q. Wu, *Angew. Chem., Int. Ed.*, 2020, **59**, 16675–16682.
23 Y. Peng, Y. Yao, L. Li, Z. Wu, S. Wang and J. Luo, *J. Mater. Chem. C*, 2018, **6**, 6033–6037.
24 C.-Y. Chai, Q.-K. Zhang, C.-Q. Jing, X.-B. Han, C.-D. Liu, B.-D. Liang, C.-C. Fan, Z. Chen, X.-W. Lei, A. Stroppa, R. O. Agbaoye, G. A. Adebayo, C.-F. Zhang and W. Zhang, *Adv. Opt. Mater.*, 2023, **11**, 2201996.
25 T. Ono, K. Ishihama, A. Taema, T. Harada, K. Furusho, M. Hasegawa, Y. Nojima, M. Abe and Y. Hisaeda, *Angew. Chem., Int. Ed.*, 2021, **60**, 2614–2618.
26 Z.-Q. Li, Z.-L. Gong, J.-Y. Shao, J. Yao and Y.-W. Zhong, *Angew. Chem., Int. Ed.*, 2021, **60**, 14595–14600.
27 K. T. Kamtekar, A. P. Monkman and M. R. Bryce, *Adv. Mater.*, 2010, **22**, 572–582.
28 M. C. Gather, A. Köhnen and K. Meerholz, *Adv. Mater.*, 2010, **23**, 233–248.
29 J.-H. Jou, S.-H. Chen, S.-M. Shen, Y.-C. Jou, C.-H. Lin, S.-H. Peng, S.-P. Hsia, C.-W. Wang, C.-C. Chen and C.-C. Wang, *J. Mater. Chem. C*, 2011, **21**, 17850–17854.
30 J. H. Jou, C. Y. Hsieh, J. R. Tseng, S. H. Peng, Y. C. Jou, J. H. Hong, S. M. Shen, M. C. Tang, P. C. Chen and C. H. Lin, *Adv. Funct. Mater.*, 2012, **23**, 2750–2757.
31 L. da Silva Candido, E. Barbosa de Brito, D. Corrêa Santos and M. d F. Vieira Marques, *J. Mater. Sci.: Mater. Electron.*, 2025, **36**, 561.
32 R. Chowdhury, M. D. Preuss, H.-H. Cho, J. J. P. Thompson, S. Sen, T. K. Baikie, P. Ghosh, Y. Boeije, X. W. Chua, K.-W. Chang, E. Guo, J. van der Tol, B. W. L. van den Bersselaar, A. Taddeucci, N. Daub, D. M. Dekker, S. T. Keene, G. Vantomme, B. Ehrler, S. C. J. Meskers, A. Rao, B. Monserrat, E. W. Meijer and R. H. Friend, *Science*, 2025, **387**, 1175–1181.
33 G. Zhang, Y. Bao, H. Ma, N. Wang, X. Cheng, Z. He, X. Wang, T. Miao and W. Zhang, *Angew. Chem., Int. Ed.*, 2024, **63**, e202401077.
34 T. Granlund, L. A. A. Pettersson, M. R. Anderson and O. Inganäs, *J. Appl. Phys.*, 1997, **81**, 8097–8104.
35 D. Barah and D. Ray, *J. Phys. D: Appl. Phys.*, 2024, **57**, 135312.
36 M. Jung, K. H. Lee, J. Y. Lee and T. Kim, *Mater. Horiz.*, 2020, **7**, 559–565.
37 Y. Zhang, T. Jing, Y. Quan, S. Ye and Y. Cheng, *Adv. Opt. Mater.*, 2022, **10**, 2200915.
38 M. Y. Wong and E. Zysman-Colman, *Adv. Mater.*, 2017, **29**, 1605444.
39 P. Fan, L. Hua, X. Lai, H.-X. Ni, W. Zhu, Y.-X. Zheng and Y. Wang, *Adv. Funct. Mater.*, 2025, **35**, 2418790.
40 C. Zhang, Z.-P. Yan, X.-Y. Dong, Z. Han, S. Li, T. Fu, Y.-Y. Zhu, Y.-X. Zheng, Y.-Y. Niu and S.-Q. Zang, *Adv. Mater.*, 2020, **32**, 2002914.
41 P.-F. Gao, Y.-Y. Jiang, H. Liu, M.-S. Zhou, T. Li, H.-R. Fu, L.-F. Ma and D.-S. Li, *ACS Appl. Mater.*, 2022, **14**, 16435–16444.
42 Z. Zhou, T. Jiang, Y. Yang, Y. Deng, M. Wang, Y. Ma, S. Liu and Q. Zhao, *Adv. Opt. Mater.*, 2023, **12**, 2302185.
43 L. Wang, H. Peng, Q. Wei, L. Kong, S. Yu, J. Cao, Q. Liang, J. Zhao and B. Zou, *Laser Photonics Rev.*, 2025, **19**, 2400856.
44 Y. Ru, L. Sui, H. Song, X. Liu, Z. Tang, S.-Q. Zang, B. Yang and S. Lu, *Angew. Chem., Int. Ed.*, 2021, **60**, 14091–14099.
45 L. Yang, J. Huang, M. Qin, X. Ma, X. Dou and C. Feng, *Nanoscale*, 2020, **12**, 6233–6238.
46 P. Li, X. Gao, B. Zhao, K. Pan and J. Deng, *Adv. Fiber Mater.*, 2022, **4**, 1632–1644.
47 X. Gao, J. Wang, K. Yang, B. Zhao and J. Deng, *Chem. Mater.*, 2022, **34**, 6116–6128.
48 H. Yang, S. Ma, B. Zhao and J. Deng, *ACS Appl. Mater.*, 2023, **15**, 13668–13677.
49 H. Zhong, B. Zhao and J. Deng, *Angew. Chem., Int. Ed.*, 2025, **64**, e202418463.
50 X. Wen, S. Du, L. Zhang and M. Liu, *Angew. Chem., Int. Ed.*, 2023, **62**, e202311816.
51 K. Akagi, T. Yamashita, K. Horie, M. Goh and M. Yamamoto, *Adv. Mater.*, 2020, **32**, 1906665.
52 J. D. Joannopoulos, P. R. Villeneuve and S. Fan, *Nature*, 1997, **386**, 143–149.
53 H. Wang, H. K. Bisoyi, L. Wang, A. M. Urbas, T. J. Bunning and Q. Li, *Angew. Chem., Int. Ed.*, 2018, **57**, 1627–1631.
54 F.-Y. Ye, M. Hu, C. Du, W. Yu, X.-P. Zhou, M. Liu and Y.-S. Zheng, *Adv. Opt. Mater.*, 2023, **11**, 2201784.

55 X. Wang, X. Gao, H. Zhong, K. Yang, B. Zhao and J. Deng, *Adv. Mater.*, 2025, **37**, 2412805.
56 M.-J. Ji, W.-L. Zhao, M. Li and C.-F. Chen, *Nat. Commun.*, 2025, **16**, 2940.
57 Z.-X. Yu, X.-W. Chen, C.-F. Chen and M. Li, *Angew. Chem., Int. Ed.*, 2025, **64**, e202507802.
58 J. Liu, B. Wang, Z. Zhang, J. Yu, X. Lü, G. Fu, W. Li and W.-Y. Wong, *J. Mater. Chem. C*, 2023, **11**, 1265–1270.
59 Y. Zhang, G. Tian, D. Li, Z. Jiang, Y. Quan and Y. Cheng, *Laser Photonics Rev.*, 2024, **18**, 2400223.
60 Y. Wang, Z.-X. Chen, Z.-Z. Huo, X.-F. Hong, S. Xing, J.-W. Xu, H.-X. Ni, L. Yuan and Y.-X. Zheng, *Adv. Opt. Mater.*, 2025, **13**, 2403242.
61 M. Mazzeo, V. Vitale, F. Della Sala, M. Anni, G. Barbarella, L. Favaretto, G. Sotgiu, R. Cingolani and G. Gigli, *Adv. Mater.*, 2005, **17**, 34–39.
62 F. Salerno, J. A. Berrocal, A. T. Haedler, F. Zinna, E. W. Meijer and L. Di Bari, *J. Mater. Chem. C*, 2017, **5**, 3609–3615.
63 D. Han, C. Li, X. Jin, J. Zhou, Y. Xu, T. Jiao and P. Duan, *Adv. Photonics Res.*, 2022, **3**, 2100287.
64 J. Liu, T. He, Z.-L. Gong, N. Liang, Y. Feng, G. Long, Y.-W. Zhong and C.-J. Yao, *Adv. Opt. Mater.*, 2024, **12**, 2302486.
65 W.-T. Xu, X. Li, P. Wu, W.-J. Li, Y. Wang, X.-Q. Xu, X.-Q. Wang, J. Chen, H.-B. Yang and W. Wang, *Angew. Chem., Int. Ed.*, 2024, **63**, e202319502.
66 P. Zhao, W.-C. Guo, M. Li, H.-Y. Lu and C.-F. Chen, *Angew. Chem., Int. Ed.*, 2024, **63**, e202409020.
67 M. Li, Z. Li, X. Peng, D. Liu, Z. Chen, W. Xie, K. Liu and S.-J. Su, *Angew. Chem., Int. Ed.*, 2025, **64**, e202420474.
68 P. Zhao, W.-C. Guo, H.-Y. Lu and C.-F. Chen, *Angew. Chem., Int. Ed.*, 2025, **64**, e202424918.

